Mottl, M.J., Davis, E.E., Fisher, A.T., and Slack, J.F. (Eds.), 1994
Proceedings of the Ocean Drilling Program, Scientific Results, Vol. 139

6. PETROLOGY OF IGNEOUS ROCKS AT MIDDLE VALLEY, JUAN DE FUCA RIDGE[1]

Debra S. Stakes[2] and James M. Franklin[3]

ABSTRACT

Leg 139 of the Ocean Drilling Program drilled igneous rock at four sites in Middle Valley: Site 855 from the eastern boundary fault of the valley; Site 856 from late mafic sills that crosscut a major sulfide deposit; Site 857 from a series of highly altered sills of variable chemistry; and Site 858 from a topographic high beneath an active site of hydrothermal discharge. The oldest rocks are from Site 855. These are N-MORBs containing refractory megacrysts of olivine, calcic plagioclase and Cr-rich clinopyroxene. The rocks have $[La/Ce]_n = 0.76–0.82$, and $[Ce/Yb]_n = 0.76–0.89$. Igneous rocks from Site 856 are relatively fresh (but more altered than those from Site 855) young sills that postdate the main phase of axial magmatism and associated hydrothermal alteration. These are some of the most primitive compositions from the northern Juan de Fuca Ridge and contain refractory megacrysts of olivine and chromian spinel, with plagioclase of intermediate compositions (slightly more sodic than those for Site 855). The rock compositions are strongly depleted in LREE, with $[La/Sm]_n = 0.28–0.29$ and $[Ce/Yb]_n = 0.37–0.39$. Samples from the chilled contacts with sediments have spurious trace element chemistry due to alteration. A topographic high drilled at Site 858 is composed of N-MORB and T-MORB lavas that must have erupted above the sediments, suggesting a relatively old age, near that of the basement. They are aphyric to slightly phyric with sodic plagioclase and magnesiochromite. Pseudomorphs of small mafic phenocrysts are inferred to be replacements of olivine. These rocks are relatively homogeneous with $[Ce/Yb]_n > 1.3$, suggesting a lower percentage of partial melting compared to the other sites. They have $[La/Ce]_n = 0.84–0.94$ and a variably developed negative Eu anomaly. The sill complex drilled at Site 857 is extensively altered. Trace elements (especially REE) suggest that they are derived from heterogeneous mantle source regions, with some mixing. One source region is similar to that of Site 855 with $[La/Ce]_n < 0.82$ and $[La/Yb]_n < 1$. The second source is similar to that of Site 858 with $[La/Ce]_n > 0.82$ and $[La/Yb]_n > 1$. Although the age relationships among the sills are difficult to constrain, the former compositions tend to be the most altered, and likely of greater age. Thus the tectonic scenario is that a robust magma chamber formed the Site 855 basalts and fed the older sills at Site 857. Magmas constructed the Site 858 topographic high and basalts from a similar mantle source region fed some of the sills at Site 857. Sills of intermediate composition suggest mixing between these magmas, either in the source region or in crustal magma chambers. The Site 856 sills postdate the ridge jump to West Valley after the Middle Valley rift failed.

INTRODUCTION

The Middle Valley segment at the northern end of the Juan de Fuca Ridge is a deep extensional rift blanketed with 200–500 meters of Pleistocene turbiditic sediment. This area was selected to be drilled during Ocean Drilling Program Leg 139 to elucidate the processes and products of hydrothermal circulation in a sedimented ridge environment (Davis, Mottl, Fisher, et al., 1992). Although Middle Valley is hydrothermally active (there are hot springs and regions of high heat flow), a relatively continuous impermeable sediment cover over zero-age crust limits the recharge and discharge of hydrothermal fluid (Davis and Villinger, 1992). This sedimentary cover also obscures the volcanic morphology and possible relationship between hydrothermal activity and specific magmatic events. More fundamental is the impact and interaction of the sediment cover on the structure and lithology of the volcanic units, transforming what would be the shallow volcanic carapace of an unsedimented ridge into a series of crystalline sills intruded into the water-rich terrigenous sediments.

During this leg, holes were successfully drilled at four sites: (1) Site 855, near the eastern boundary fault; (2) Site 856, a topographic high with massive sulfide deposits; and a central area with (3) Site 857, high heat flow, and (4) Site 858, active hot springs (Davis, Mottl, Fisher, et al., 1992) (Fig. 1). The latter two sites are reentry sites and form a suite of drilled samples from an active spreading center hydrothermal zone. This paper describes the petrology of igneous rocks from these four sites. At Site 855, only a few samples of MORB-type basalt, thought to represent the basement to Middle Valley during its early rifting stages, were obtained. Site 856 has a few thin sills of primitive picritic basalt. Site 857 intersected numerous mafic sills. At Site 858, a constructional high built of moderately evolved basalt and basaltic andesitic was discovered beneath 250 m of altered sediments at the area of high-temperature active venting. Samples from each of these four suites are thus treated separately in the present report with the mineralogical data presented first, followed by chemical data. Although a detailed description of the hydrothermal alteration is not provided here (Stakes, unpubl. data), a summary of the relative impact of alteration on whole-rock chemical variation is provide for each site. The results of this study demonstrate the nature of primary magmatic variation in a ridge setting, where mafic sill complexes make up much of the volcanic stratigraphy and younger seamounts or primitive magmas provide evidence of variable melting conditions beneath a rift with waning magmatic activity.

ANALYTICAL METHODS

Mineral Chemistry and Petrography

The results presented here are based on detailed petrographic examination of over 200 polished thin sections followed by detailed electron microprobe studies. Microprobe facilities at the University of South Carolina (silicates, spinels) and the Geological Survey of Canada (sulfides, iron oxides) were used. Instruments at both institutions are fully automated Cameca SX-50 electron microprobe systems with on-line mineral formula calculations based on stoichiometry (spinel, plagioclase, olivine). All phases were analyzed with a focused beam (2–3 microns beam size), 15 kV accelerating voltage and ZAF on line correction. A minimum of four analyses was obtained for each grain including multiple analyses of cores and rims to determine zonation. Pyroxene formulas were calculated using the algorithms of Papike et al. (1974). A combination of artificial and mineral standards are used by each facility. Results of microprobe analyses are presented in Table

[1] Mottl, M.J., Davis, E.E., Fisher, A.T., and Slack, J.F. (Eds.), 1994. *Proc. ODP, Sci. Results*, 139: College Station, TX (Ocean Drilling Program).
[2] Monterey Bay Aquarium Research Institute, 160 Central Avenue, Pacific Grove, CA 93950, U.S.A.
[3] Geological Survey of Canada, 601 Booth Street, Ottawa, K1AOE8, Canada.

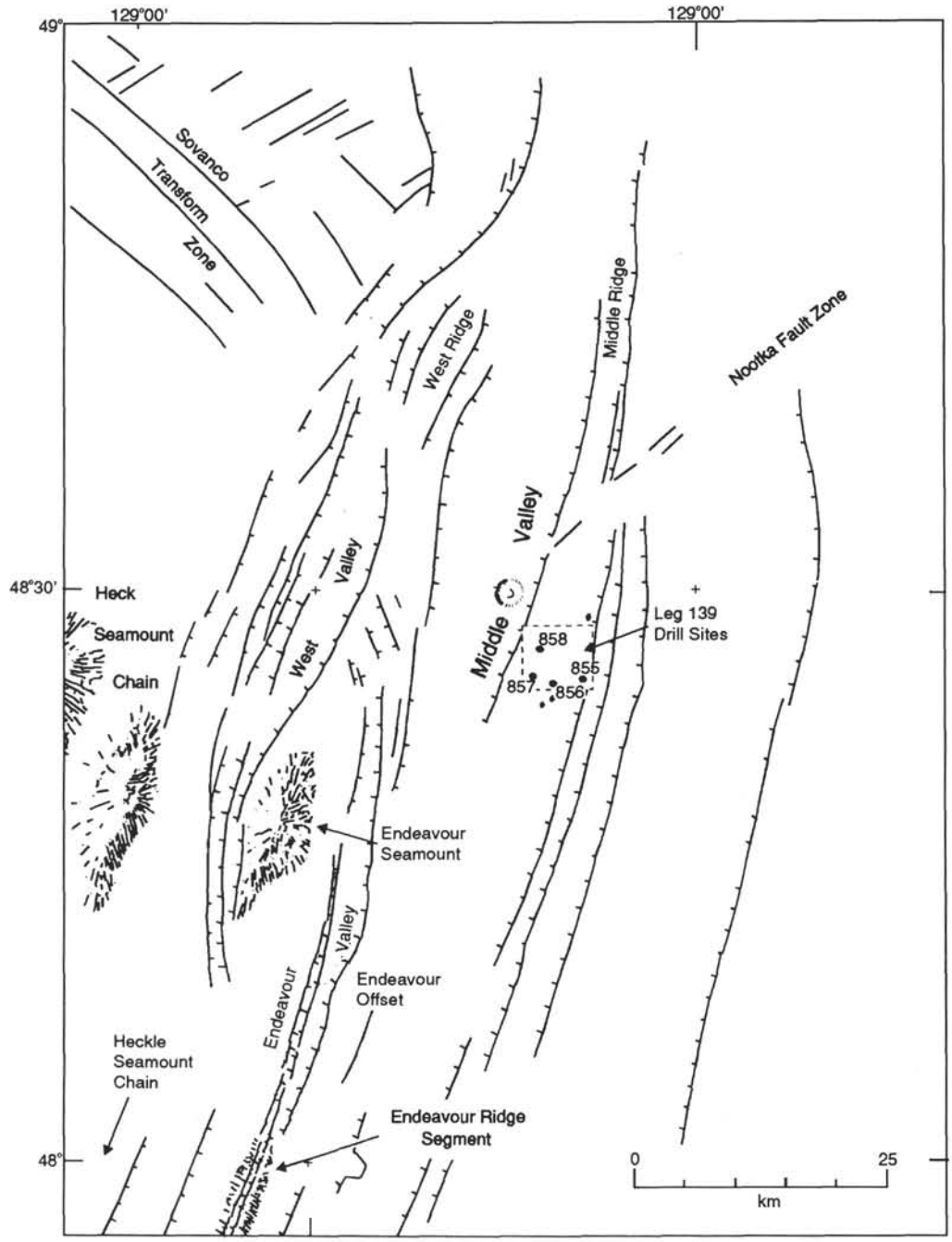

Figure 1. Regional map showing main tectonic features, after Davis and Villinger (1992).

3 (olivine), Table 4 (plagioclase), Table 5 (pyroxene), Table 6 (spinel), Table 7 (magnetite-ilmenite) and Table 8 (sulfide).

Detailed lithostratigraphy and estimates of recovery for all igneous rocks are presented in the Leg 139 *Initial Reports* volume (Davis, Mottl, Fisher, et al., 1992) and will only be summarized here. The petrographic descriptions presented here supplement the shipboard reconnaissance examination of thin sections, which includes sizes of phenocrysts and modal proportions.

Major and Trace Element Analyses

Major oxides and some minor and trace elements were determined by fused disk X-ray fluorescence (XRF) at the Geological Survey of Canada. Trace elements including Ag, Ba, Be, Co, Cr, Cu, Ni, Pb, Sc, Sr, V, Zn, and Zr were determined using Inductively-Coupled Plasma Emission Spectrometry (ICP-ES). The rare earth elements, as well as Y, were also determined using inductively-coupled Plasma Mass Spectrometry (ICP-MS), using a total dissolution method (perchloric, nitric, hydrofluoric acids). Combustion and wet chemical methods were used to determine FeO, total H_2O (=H_2OT), total CO_2 (=CO_2T) and total sulfur (=ST). Where listed, FeO is the wet chemistry determinations. Total iron (Fe_2O_3T) was determined by XRF assuming total oxidation on combustion. FeO is determined by titration and Fe_2O_3 is calculated by difference. Values for the Mg number (=Mg/Mg+Fe^{+2} on a molecular basis) are calculated using Fe^{+2} = 0.9 (Fe Total) (=Mg#) and the value for Fe_2O_3T (=$Mg\#^*$). Detection limits and precision data are available on request to JMF. Data from the shipboard analyses (Davis, Mottl, Fisher, et al., 1992) are also considered where appropri-

ate. In particular, the shipboard analysis for Nb is used for comparison with previous work as it is more consistent with other laboratories and previous work in the classification of the basalts. These values are at the detection limit for XRF analysis. In general, however, the data set obtained for this study (Table 1) is considered to be slightly more precise than that for the shipboard analyses, due to more precise weighing.

Alteration of the igneous rocks within an active hydrothermal area can substantially modify whole-rock compositions and obscure primary mineralogy. For each site, we provide an overview of the alteration of the rocks and the extent to which this alteration could have biased the chemical parameters used for igneous petrochemistry. Petrographic observations and oxygen isotope analyses are used to discriminate alteration. Total hydrous alteration can be inferred from total H_2O. That much of the alteration is nonoxidative can be inferred from the measured values for FeO. The impact of sulfide mineralization can be inferred from the values of total sulfur.

Oxygen Isotope Analyses

Whole-rock powders from shipboard and land-based chemical analyses were analyzed for oxygen isotopes at the University of South Carolina (Table 2). Oxygen isotopes are one of the most sensitive indicators of seawater hydrothermal alteration and are a useful index of alteration. Twelve milligrams of each powder were weighed and dried in a 100°C furnace prior to loading onto the extraction line. Samples were reacted with ClF_3 to liberate pure oxygen gas, which was then converted to CO_2 by reaction with a hot carbon rod. The CO_2 was analyzed for its isotopic composition on a SIRA mass spectrometer. Results are reported in the standard δ-notation.

REGIONAL SETTING

The magmatic history of the northern Juan de Fuca ridge is complicated by ridge propagation and the influence of the adjoining Heck and Heckle Seamount Chain (Fig. 1). The former of these intersects the ridge at the Endeavour Seamount, where the southern end of West Valley and the northern end of the Endeavour Ridge form an overlapping spreading center separated by the Endeavour Offset (Fig. 1). Previous studies suggest that the West Valley segment is propagating to the south while the Endeavour Segment is undergoing ridge failure (Karsten et al., 1990). Middle Valley was the axis of active spreading for the northern Juan de Fuca Ridge prior to approximately 200,000 yr ago. Sometime in the last 200,000 yr and perhaps as recently as 20,000 to 10,000 yr ago, spreading was initiated in West Valley, 20 km to the west. Active spreading slowed in Middle Valley during this period, especially during the last 10,000 yr (Mottl, Davis, Fisher, et al., 1992). Middle Valley is now bounded by West Ridge and Middle Ridge, which are presumed to have been constructed at the Middle Valley spreading center when it was active. Lavas of primitive compositions have been previously described for West Ridge, whereas West Valley has both primitive (southern end) and evolved compositions (central and northern ends), consistent with ridge propagation to the south (Van Wagoner and Leybourne, 1991). Rocks from the West Valley segment include a large range of variation, explained by (1) heterogeneous mantle, (2) mixing of mantle source domains, and (3) mixing within crustal magma chambers (Van Wagoner and Leybourne, 1991). The Endeavour Segment, which is dominated by compositions slightly more enriched compared to mid-ocean ridge basalt, has secular compositional heterogeneity. The dominance of enriched compositions for the Endeavour Segment has been attributed to reduced melting of an enriched mantle beneath this region associated with the waning stages of this failing segment (Karsten et al., 1990) or due to recent introduction of enriched mantle (Michael et al., 1989). In contrast, the Heck and Heckle Seamount chains are highly depleted, have a restricted range of incompatible elements and are distinct from the adjacent West Valley (Leybourne and Van Wagoner, 1991). Rocks recovered by drilling in Middle Valley can thus be compared to the broadly variable compositions in adjacent tectonic domains to test the model of rift failure, temporal variability, and timing of mantle enrichment for the northern portion of the Juan de Fuca Ridge.

Site 855

Setting

At Site 855 igneous rock was recovered from the base of each of a series of four drillholes intended to transect the hanging wall and footwall of the eastern boundary fault. Each of these drillholes penetrated less than 20 m into basement; only a few pieces of fresh porphyritic basalt flows were recovered at the bottom of each hole (Davis, Mottl, Fisher, et al., 1992). Pieces recovered include abundant fresh glass and large phenocrysts of olivine, plagioclase, and clinopyroxene. Some samples have microcrystalline groundmass minerals with variolitic or skeletal textures. The groundmass minerals, in general, have more evolved compositions than the larger phenocrystic minerals. No spinel was observed in any of the samples. Virtually no sulfide was observed in these basalt samples. Fe-oxide was present as a discrete phase only in the more crystalline specimens. Alteration is limited to low-temperature phases such as smectite, celadonite and carbonate, except for rare replacement of olivine by talc or chlorite. The bulk oxygen isotopic values (7.0 to 8.0‰) are higher than fresh MORB (5.8‰; Ito et al., 1987) as a result of the presence of the low temperature phases. Plagioclase phenocrysts will also increase the $\delta^{18}O$ of the powder.

Petrography And Mineral Chemistry

Olivine phenocrysts tend to be large and rounded to euhedral with rare normal compositional zonation. Some crystals are intergrown with megacrysts of plagioclase or clinopyroxenes to form glomerocrysts. The average composition is Fo_{83} with a range from Fo_{77-86} (Table 3).

Plagioclase phenocrysts from Hole 855A have compositions ranging from calcic cores of An_{88} to more sodic rims of An_{76} (Table 4). Phenocrysts from Hole 855D are slightly more sodic in composition, from An_{74-68}. The phenocrysts are euhedral columnar crystals of various sizes that are rarely embayed. Many of the large crystals have abundant inclusions of fresh glass. Most of the larger crystals have oscillatory zoning. Some groundmass plagioclases are skeletal with lantern shapes, but most are lathlike and in radiating aggregates with pyroxene. These small crystals have average compositions of An_{70-75} with some rims as sodic as An_{58} (Table 4).

Clinopyroxene phenocrysts are elongate and rounded, frequently twinned, and are included in glomerocrystic aggregates with plagioclase. The large megacrysts (1–4 mm) are relatively high in Al contents (>3.5% Al_2O_3) and Cr contents (>1% Cr_2O_3) (Table 5), characteristics typically associated with high pressure crystallization (Basaltic Volcanism Study Project, 1981). Some of these large crystals poikilitically enclose plagioclase crystals. Like some olivines, the clinopyroxene megacrysts display rims with smaller groundmass phases nucleating on the rounded grain boundaries. Smaller clinopyroxene microphenocrysts and rims on zoned crystals have higher Ti and Fe, lower Cr, and lower Al (Table 5) than the large megacrysts. Some smaller clinopyroxenes form "bowtie" intergrowths with laths of plagioclase, or are small barrel-shaped crystals.

Major Elements

The samples are all very fine-grained to cryptocrystalline or glassy basalt. Alteration is not pronounced and these samples have the lowest volatile contents of any of the suites examined in this study. The three samples analyzed as part of this study are similar to those reported in the Leg 139 Shipboard Report (Davis, Mottl, Fisher, et al., 1992). The major and trace elements (Table 1) indicate that the samples are moderately fractionated abyssal tholeiite. On the Mg-number variation diagrams (Fig. 2), the data are linearly distributed, as expected for frac-

Table 1. Composition of igneous rocks from Sites 855, 856, and 858, Middle Valley area.

A. Major elements

Core, section, interval (cm)	Depth (mbsf)	SiO_2	TiO_2	Al_2O_3	$Fe_2O_3^t$	Fe_2O_3	FeO	MnO	MgO	CaO	Na_2O	K_2O	H_2O^t	CO_2^t	P_2O_5	TOTAL	Mg#	Mg#*
139-855A-																		
8R-1, 18–20	65.0	49.50	1.66	15.70	10.80	2.80	7.20	0.20	7.82	12.00	2.40	0.16	0.3	0.30	0.17	100.40	0.61	0.59
9R-1, 46–48	74.8	49.70	1.45	15.20	9.90	2.70	6.50	0.16	7.68	12.10	2.80	0.12	0.8	0.30	0.12	99.80	0.63	0.61
139-855D-																		
6R-1, 40–42	114.3	49.70	1.57	14.20	11.30	2.60	7.80	0.19	7.69	11.90	2.50	0.12	0.7	0.40	0.13	99.80	0.60	0.57
139-856A-																		
14X-1, 90–92	115.4	47.70	0.84	15.90	8.80	2.60	5.60	0.15	11.20	11.60	1.90	0.05	2.6	0.20	0.05	100.70	0.74	0.72
14X-1, 7–9	115.9	47.60	0.83	15.80	8.90	2.20	6.00	0.15	11.40	11.70	1.90	0.05	2.3	0.20	0.05	100.50	0.74	0.72
14X-CC, 9–11	114.6	47.10	0.81	15.60	8.90	2.20	6.00	0.14	12.40	10.50	1.80	0.05	3.1	0.10	0.05	100.10	0.75	0.73
139-856B-																		
10H-1, 64–67	71.4	47.10	0.86	16.30	8.20	2.20	5.40	0.12	11.40	9.60	2.00	0.02	3.1	0.40	0.06	98.90	0.75	0.73
10H-1, 93–95	71.7	45.80	1.13	20.80	5.30	0.90	4.00	0.04	8.37	6.56	2.50	0.02	6.9	0.10	0.04	98.20	0.78	0.76
10H-2, 9–12	72.4	46.30	0.86	16.20	8.20	2.60	5.00	0.11	11.70	9.23	1.90	0.02	3.8	0.30	0.05	98.40	0.76	
139-857C-																		
59R-1, 131–133	472.4	50.00	1.62	15.00	9.40	1.50	7.10	0.19	7.52	12.20	2.30	0.02	1.7	0.10	0.18	100.00	0.64	0.61
59R-2, 62–64	473.2	50.30	1.62	15.30	9.20	1.20	7.20	0.17	7.61	12.10	2.30	0.02	1.8	0.10	0.18	100.20	0.65	0.62
59R-2, 94–96	473.5	49.80	1.65	14.70	10.00	1.60	7.60	0.18	7.93	12.20	2.20	0.02	2.0	0.20	0.18	100.50	0.64	0.61
59R-3, 40–42	69.9	50.50	1.68	14.70	9.00	1.10	7.10	0.17	8.22	12.40	2.30	0.02	1.8	0.10	0.18	100.50	0.67	0.64
59R-3, 117–119	475.2	50.90	1.53	14.50	8.40	0.80	6.80	0.16	8.05	11.90	2.10	0.02	2.1	0.20	0.16	99.40	0.68	0.65
59R-4, 35–37	475.9	51.50	1.55	15.20	7.90	1.20	6.00	0.17	7.60	12.10	2.40	0.02	1.6	0.20	0.17	99.90	0.68	0.66
59R-4, 111–113	476.6	49.30	1.58	15.20	9.70	1.60	7.30	0.22	7.27	11.90	2.30	0.02	2.0	0.10	0.17	100.60	0.65	0.63
60R-1, 32–34	481.1	47.50	1.61	15.00	10.20			0.25	7.72	12.40	2.30	0.02			0.17	100.00	0.62	0.60
60R-1, 75–77	481.6	49.60	1.61	14.70	9.40			0.19	7.56	12.30	2.30	0.02		0.10	0.17	99.70	0.64	0.61
60R-1, 173–175	482.5	48.20	1.61	15.40	9.50	1.30	7.40	0.22	8.29	12.50	2.30	0.02	2.1		0.17	100.30	0.66	0.63
60R-2, 12–14	482.3	47.90	1.57	15.10	10.20			0.22	7.60	12.30	2.40	0.02			0.17	99.90	0.62	0.60
60R-2, 28–30	482.5	46.10	1.85	16.10	9.10	1.00	7.30	0.24	10.40	9.20	2.80	0.02	3.9	0.10	0.20	99.50	0.72	0.69
61R-1, 32–34	490.8	47.80	1.43	14.40	12.20			0.24	10.10	8.19	1.60	0.02		0.10	0.15	98.20	0.65	0.62
61R-2, 4–6	491.9	44.50	1.56	16.40	9.90	1.70	7.40	0.31	12.50	5.60	2.20	0.02	6.2	0.10	0.14	99.70	0.74	0.71
62R-1, 20–22	500.2	48.20	1.26	15.10	10.60			0.26	10.10	7.92	1.80	0.02		0.10	0.12	96.80	0.68	0.65
62R-1, 67–69	500.7	48.00	1.03	15.60	11.60			0.25	7.59	10.30	1.20	0.02		0.10		97.60	0.59	0.56
62R-2, 7–9	501.6	47.90	0.92	15.60	7.30	1.10	5.60	0.24	11.80	9.80	2.30	0.02	3.8	0.10	0.07	99.40	0.78	0.76
62R-2, 50–52	502.0	48.60	1.53	16.60	7.80	1.10	6.00	0.27	9.27	10.00	2.60	0.02	2.3		0.14	98.90	0.72	0.70
63R-1, 38–40	510.1	49.20	1.35	15.50	9.50	1.30	7.40	0.29	9.70	9.38	2.00	0.02	3.4	0.10	0.13	100.00	0.69	0.67
63R-1, 69–71	510.4	47.30	1.51	15.90	9.50	1.30	7.40	0.24	9.36	11.50	1.90	0.02	2.7		0.14	99.70	0.68	0.66
64R-1, 13–15	519.5	53.50	1.30	14.50	8.70			0.21	7.07	9.23	2.00	0.02		0.10	0.12	98.50	0.64	0.62
64R-1, 112–114	520.5	48.90	1.36	15.50	9.40	1.40	7.20	0.24	8.47	12.20	2.10	0.02	2.1	0.10	0.13	100.70	0.66	0.64
64R-2, 74–76	521.6	44.60	1.63	15.20	12.30	1.60	9.60	0.30	11.10	9.31	1.50	0.02	4.3		0.14	99.80	0.67	0.64
66R-1, 94–96	539.3	45.90	2.08	15.30	11.20	1.90	8.40	0.22	8.34	11.30	1.80	0.02	3.1	0.10	0.24	99.50	0.62	0.60
66R-1, 122–124	540.0	47.50	2.05	15.70	10.20			0.21	7.27	11.60	2.20	0.02		0.10	0.23	98.30	0.61	0.59
67R-1, 73–75	549.1	47.50	1.53	15.70	10.40	1.50	8.00	0.31	8.91	11.30	1.60	0.02	2.9	0.10	0.14	99.70	0.65	0.63
68R-1, 12–14	558.1	45.90	1.56	16.80	11.80	1.70	9.10	0.38	9.18	9.21	1.50	0.02	3.9	0.10	0.16	100.10	0.63	0.61
68R-1, 90–92	558.9	47.80	1.52	15.90	10.10	1.30	7.90	0.35	9.29	11.40	1.60	0.02	2.8	0.10	0.15	100.40	0.67	0.65
68R-2, 28–30	559.8	47.70	1.71	15.90	10.10	1.40	7.80	0.33	8.46	11.60	1.70	0.02	2.5		0.17	100.00	0.65	0.62
68R-2, 72–74	560.2	45.40	1.73	17.10	11.00	1.40	8.60	0.39	9.04	10.00	1.60	0.02	3.6	0.10	0.18	99.60	0.64	0.62
68R-3, 11–13	561.1	47.60	1.52	15.70	10.10	2.10	7.20	0.31	9.70	10.10	1.50	0.02	3.9	0.10	0.14	100.00	0.68	0.66
139-857D-																		
3R-1, 117–120	600.5	38.40	1.73	18.50	15.30	2.40	11.60	0.35	12.30	6.08	1.30	0.02	6.9	0.10	0.15	100.40	0.64	0.61
4R-1, 138–140	610.3	37.40	1.11	18.20	18.00			0.45	12.80	4.49	0.80	0.02		0.10	0.08	95.60	0.61	0.58
8R-1, 96–98	648.3	50.10	2.27	13.70	11.70	1.50	9.20	0.24	6.74	10.90	2.20	0.02	2.2	0.10	0.20	100.00	0.56	0.53
12R-1, 88–90	686.8	43.70	1.44	16.60	11.60	1.90	8.70	0.35	14.20	3.92	0.20	0.02	8.4	0.10	0.13	100.40	0.73	0.71
24R-1, 115–117	802.4	49.70	1.40	15.80	9.70	1.70	7.20	0.21	7.83	11.60	2.20	0.02	1.8		0.15	100.50	0.64	0.62
24R-2, 64–66	803.3	48.10	1.41	15.90	8.80	2.70	5.50	0.22	8.07	14.10	2.30	0.02	1.6		0.15	100.30	0.67	0.64
24R-2, 114–116	803.8	48.30	1.38	15.40	8.50			0.20	8.15	14.30	2.10	0.02			0.15	99.80	0.68	0.66
24R-3, 24–26	804.3	50.40	1.37	15.60	8.40	1.50	6.20	0.18	7.57	12.10	2.50	0.02	1.7		0.14	100.40	0.66	0.64
25R-1, 64–66	811.4	49.50	1.39	15.80	9.40	2.50	6.20	0.17	7.77	12.10	2.30	0.02	2.0		0.14	100.10	0.65	0.62
26R-1, 76–78	821.1	49.50	1.38	15.40	9.50			0.20	7.64	12.00	2.40	0.02			0.15	99.40	0.64	0.61
32R-1, 58–61	878.7	49.20	1.96	14.80	11.20	1.80	8.50	0.23	7.38	11.90	2.30	0.02	2.0	0.10	0.19	100.60	0.59	0.57
36R-1, 74–76	917.6	49.00	2.05	13.90	12.30	2.90	8.50	0.22	6.68	11.50	2.10	0.02	2.2	0.10	0.17	100.20	0.54	0.52
139-858F-																		
25R-1, 118–119	250.1	45.10	1.76	17.30	10.30			0.21	11.00	3.03	4.30	0.02		0.20	0.18	96.40	0.70	0.68
26R-1, 42–44	259.0	48.30	1.52	15.50	9.30	1.90	6.70	0.14	7.65	12.40	2.50	0.02	2.3	0.20	0.17	99.80	0.64	0.62
27R-1, 42–43	268.2	48.90	1.55	16.30	9.70	2.60	6.40	0.15	7.50	12.80	2.80	0.02	1.4	0.20	0.17	101.00	0.63	0.60
29R-1, 63–65	287.8	48.80	1.61	15.70	8.70	1.50	6.50	0.15	8.64	10.80	3.40	0.02	2.5	0.10	0.17	100.10	0.69	0.66
139-858G-																		
1R-1, 37–39	277.2	47.70	1.60	16.10	9.60	1.80	7.00	0.15	8.50	11.10	2.90	0.02	2.8	0.10	0.18	100.80	0.66	0.64
2R-1, 53–55	287.0	48.60	1.51	15.20	8.90	2.60	5.70	0.17	7.72	12.60	2.80	0.02	2.3	0.10	0.17	99.70	0.66	0.63
3R-1, 24–25	296.3	48.80	1.54	15.60	9.20	2.10	6.40	0.16	7.94	12.10	3.10	0.02	2.4	0.20	0.17	100.80	0.66	0.63
4R-1, 26–28	306.1	49.60	1.54	15.50	9.00	2.20	6.10	0.15	7.73	12.50	3.00	0.02	2.1	0.20	0.17	101.10	0.65	0.63
4R-1, 71–73	306.5	48.50	1.55	15.50	9.20	1.60	6.80	0.16	7.72	13.00	2.70	0.02	1.8		0.17	100.00	0.65	0.62
8R-1, 36–38	344.9	49.10	1.52	15.60	9.30			0.19	7.90	12.30	2.60	0.02	2.0	0.10	0.17	101.10	0.65	0.63
7R-1, 33–35	335.1	48.90	1.59	15.30	8.90	1.70	6.50	0.21	8.15	11.60	3.30	0.02	2.4	0.10	0.17	100.10	0.67	0.64
6R-1, 29–32	325.4	47.80	1.54	15.50	9.00	1.40	6.80	0.22	8.70	12.10	2.70	0.02	2.4	0.20	0.17	100.10	0.68	0.66
5R-1, 16–18	315.6	47.40	1.54	15.80	10.50			0.15	7.52	12.40	2.70	0.02		0.10	0.16	99.80	0.61	0.59
10R-1, 31–33	365.2	48.40	1.50	15.10	9.70			0.16	7.90	12.20	2.50	0.02		0.10	0.16	99.00	0.64	0.62
10R-1, 104–106	365.9	48.40	1.58	15.80	9.10	1.40	6.90	0.15	7.89	12.60	2.80	0.02	1.5		0.17	100.10	0.66	0.63
11R-1, 13–15	374.6	49.90	1.55	15.20	8.90	1.60	6.60	0.16	7.31	12.90	3.00	0.02	1.6	0.10	0.17	100.30	0.64	0.62
12R-1, 48–50	384.7	46.90	1.53	15.50	10.70			0.14	7.07	12.70	2.70	0.02		0.10	0.16	99.70	0.59	0.57
13R-1, 9–11	394.0	48.20	1.60	16.00	9.60	1.30	7.50	0.16	7.53	12.30	2.50	0.02	2.1		0.17	99.70	0.63	0.61
13R-1, 25–27	394.2	47.90	1.57	15.50	9.70	1.60	7.30	0.15	7.58	12.80	2.50	0.02	1.7		0.17	99.70	0.63	0.61
14R-1, 41–43	404.0	48.40	1.56	15.60	8.90	2.20	6.00	0.15	7.30	13.00	2.60	0.02	2.2	0.10	0.17	99.50	0.64	0.62
15R-1, 31–33	413.6	47.30	1.62	16.40	9.70	2.10	6.80	0.16	7.01	13.20	2.70	0.02	1.8		0.18	100.30	0.61	0.59
16R-1, 77–79	423.7	49.40	1.58	14.00	9.70			0.17	8.00	10.50	3.30	0.02		0.10	0.16	98.40	0.64	0.62

Notes: Fe_2O_3t = total Fe as Fe^{3+} assuming total oxidation on combustion. Mg# = Mg/Mg + Fe^{2+} on a molecular basis where where Fe^{2+} = 0.9(Fe total). Mg#* = Mg# where Fe^{2+} = Fe total. All analyses by fused disk X-ray fluorescence except H_2O and CO_2 by combustion.

tionation. On a CaO/Al_2O_3 vs. Mg# diagram, they fall within the range of the Endeavour Segment samples (Davis, Mottl, Fisher, et al., 1992).

Trace Elements

Basalts can be classified as enriched mid-ocean ridge basalt (E-MORB), transitional mid-ocean ridge basalt (T-MORB) or normal

Table 1 (continued).

B. Minor and trace elements

Core, section, interval (cm)	St	Ba	Be	Co	Cr	Cu	La	Nb	Ni	Pb	Sc	Sr	V	Y	Yb	Zn	Zr	Ce	Dy	Er	Eu	Gd	Ho	Nd	Sm	Tm	Zr/Y	$[La/Ce]_n$	$[La/Sm]_n$
139-855A-																													
8R-1, 18–20	0.08	40	0.6	44	240	68	3.8	13	140		34	110	280	40	4.4	98	110	13	6.7	4.1	1.4	6.0	1.5	12	4.4	0.6	0.39	0.76	0.54
9R-1, 46–48	0.08	80	0.6	43	230	68	3.8	13	100		37	140	260	32	3.5	81	87	12	5.4	3.3	1.3	5.0	1.3	10	3.6	0.5	0.33	0.83	0.66
139-855D-																													
6R-1, 40–42	0.16	40	0.6	43	200	64	3.5	12	77		40	130	290	36	4.0	87	96	12	6.3	3.7	1.4	5.6	1.4	11	3.8	0.6	0.33	0.76	0.58
139-856A-																													
14X-1, 90–92	0.09	60		42	560	69	0.9	15	250		28	63	170	21	2.4	80	33	3.4	3.7	2.2	0.8	3.2	0.8	4.5	1.9	0.4	0.19	0.65	0.28
14X-1, 7–9	0.14	50		42	550	66	0.9	13	240		28	64	170	22	2.3	69	34	3.5	3.6	2.3	0.8	3.1	0.8	4.6	2.0	0.3	0.20	0.70	0.30
14X-CC, 9–11	0.14	30		49	610	74	0.9	11	300		28	60	170	21	2.3	62	31	3.4	3.6	2.1	0.8	3.0	0.8	4.5	1.9	0.3	0.18	0.67	0.29
139-856B-																													
10H-1, 64–67	0.12	60		43	540	73	1.2	11	260	22	28	77	170	21	2.4	87	35	3.9	3.6	2.3	0.9	3.3	0.9	4.7	2.0	0.4	0.21	0.80	0.38
10H-1, 93–95	0.75	80	0.5	62	810	180	1.6	5	380	22	37	88	220	8.6	1.7	62	46	3.2	2.0	1.4	0.6	1.6	0.5	2.6	1.1	0.2	0.21	1.30	0.92
10H-2, 9–12	0.14	60		42	580	66	0.9	5	260		27	69	160	21	2.3	75	32	3.4	3.6	2.2	0.8	3.0	0.8	4.6	1.9	0.3	0.20	0.69	0.30
139-857C-																													
59R-1, 131–133	0.07	30	0.7	37	280	81	6.1	13	76		37	210	260	32	3.2	69	130	18	5.5	3.3	1.5	5.5	1.2	14	4.2	0.5	0.50	0.88	0.91
59R-2, 62–64	0.39	60	0.8	32	270	58	6.4	14	76		37	220	250	31	3.2	74	130	18	5.6	3.2	1.5	5.5	1.2	14	4.2	0.5	0.52	0.93	0.96
59R-2, 94–96	0.10	80	0.8	35	260	54	6.4	13	75		37	200	250	32	3.3	79	130	19	5.6	3.3	1.5	5.8	1.3	15	4.2	0.5	0.52	0.88	0.96
59R-3, 40–42	0.18	60	0.8	33	280	67	6	13	69		40	200	250	32	3.4	78	130	18	5.9	3.4	1.5	5.8	1.3	14	4.1	0.5	0.52	0.87	0.92
59R-3, 117–119	0.03	30	0.7	32	280	53	5.7	5	84		34	200	220	29	2.9	64	120	17	5.1	3.1	1.5	5.1	1.1	13	3.8	0.4	0.55	0.87	0.94
59R-4, 35–37	0.02	70	0.7	26	270	80	5.7	12	81		36	220	230	30	3.1	59	130	17	5.3	3.1	1.5	5.2	1.1	13	4.0	0.5	0.57	0.87	0.90
59R-4, 111–113	0.44	40	0.7	32	260	120	6.4	14	79		35	210	230	30	3.2	71	130	18	5.4	3.3	1.5	5.6	1.2	14	4.0	0.5	0.57	0.93	1.01
60R-1, 32–34	2.65	50	0.8	37	250	41	5.8	11	73		37	210	240	31	3.4	49	130	17	5.7	3.2	1.5	5.5	1.2	14	4.1	0.5	0.54	0.89	0.89
60R-1, 75–77	1.59	70	0.8	36	240	84	5.8	12	72		37	210	240	31	3.4	48	130	18	5.6	3.3	1.5	5.6	1.2	14	4.1	0.5	0.54	0.84	0.89
60R-1, 173–175	0.63	60	0.7	31	270	91	6	5	75	70	37	200	240	30	3.2	350	130	18	5.6	3.2	1.5	5.6	1.2	14	4.2	0.5	0.54	0.87	0.90
60R-2, 12–14	2.28	50	0.7	38	250	50	6.4	12	85		37	210	240	31	3.4	52	120	18	5.5	3.3	1.5	5.5	1.2	14	4.1	0.5	0.50	0.93	0.98
60R-2, 28–30	0.12	70	1.2	32	310	14	6	5	81		42	210	260	30	3.2	77	140	18	5.5	3.2	1.3	5.5	1.2	14	4.1	0.5	0.54	0.87	0.92
61R-1, 32–34	1.79	50	0.8	46	230	37	6.2	14	79		32	140	210	26	2.9	86	110	17	4.7	2.8	1.3	4.7	1.0	12	3.6	0.4	0.52	0.95	1.08
61R-2, 4–6	0.90	70	1.3	32	310	5	3.8	5	90		39	140	240	31	3.4	180	110	13	5.5	3.3	1.3	5.5	1.2	11	3.7	0.5	0.46	0.76	0.65
62R-1, 20–22	1.13	80	0.5	39	250	79	3.5	11	84		31	180	190	26	2.7	89	88	11	4.7	2.7	1.5	4.5	1.0	10	3.3	0.4	0.46	0.82	0.67
62R-1, 67–69	1.80	70	0.5	36	190	17	3.4	5	74		26	140	220	23	2.4	140	75	10	3.9	2.3	1.7	3.9	0.9	8.4	2.7	0.4	0.34	0.89	0.79
62R-2, 7–9	0.03	30		30	360	5	1.7	12	83		43	160	180	18	2.0	87	52	6.1	3.3	1.9	0.8	3.0	0.7	6	2.1	0.3	0.29	0.73	0.51
62R-2, 50–52	0.33	60	0.6	29	310	84	3.7	5	91		38	180	220	29	3.1	84	110	12	5.0	3.0	1.2	4.8	1.2	11	3.6	0.4	0.50	0.80	0.55
63R-1, 38–40	0.07	50	0.7	32	300	21	4.1	5	93		35	140	210	27	3.0	110	87	12	4.7	2.8	1.1	4.7	1.1	10	3.4	0.4	0.41	0.89	0.76
63R-1, 69–71	0.25	80	0.7	27	340	34	4.5	5	84		40	140	240	30	3.3	74	100	14	5.4	3.2	1.2	5.3	1.2	12	3.9	0.5	0.42	0.84	0.73
64R-1, 13–15	1.58	50	0.6	35	280	21	4.1	14	81	33	34	150	210	26	2.7	190	90	12	4.6	2.6	1.2	4.3	1.0	10	3.2	0.4	0.43	0.89	0.81
64R-1, 112–114	0.83	50	0.7	30	300	79	4.2	13	85		37	150	220	28	2.9	110	92	13	4.9	2.8	1.2	4.6	1.1	11	3.6	0.5	0.42	0.84	0.73
64R-2, 74–76	0.31	40	0.7	30	310	78	4.3	11	86		39	110	250	30	3.2	100	100	13	5.4	3.1	1.1	5.1	1.2	11	3.7	0.5	0.40	0.86	0.73
66R-1, 94–96	0.62	70	0.9	39	240	63	9.1	15	120		35	150	260	39	4.3	99	150	24	7.0	4.1	1.7	6.7	1.5	17	5.3	0.6	0.58	0.99	1.08
66R-1, 122–124	1.05	70	0.8	53	240	130	8.9	20	120		34	170	260	37	4.1	80	150	24	6.6	3.9	1.7	6.6	1.5	17	5.1	0.6	0.58	0.97	1.10
67R-1, 73–75	0.02	40	0.9	36	270	100	5.5	16	98		35	120	260	31	3.3	78	97	15	5.3	3.2	1.2	5.1	1.2	12	3.6	0.5	0.37	0.96	0.96
68R-1, 12–14	0.46	60	0.7	35	280	220	6.6	12	100		36	110	260	32	3.6	100	97	17	5.7	3.5	1.2	5.4	1.3	12	3.8	0.5	0.37	1.01	1.09
68R-1, 90–92	0.08	50	0.7	33	280	130	5.7	14	100		34	110	250	31	3.4	80	97	16	5.6	3.4	1.2	5.3	1.3	12	3.7	0.5	0.39	0.93	0.97
68R-2, 28–30	0.51	60	0.7	36	260	180	6.3	5	96		36	130	270	34	3.7	86	110	17	6.0	3.6	1.3	5.8	1.3	13	4.0	0.6	0.41	0.97	0.99
68R-2, 72–74	0.22	80	0.7	36	180	240	6.8	19	110		33	120	260	35	3.8	97	120	18	6.2	3.8	1.3	5.9	1.3	14	4.4	0.6	0.46	0.99	0.97
68R-3, 11–13	0.01	15	0.8	36	290	44	5.4	10	100	23	36	110	260	31	3.4	140	97	15	5.3	3.2	1.2	5.0	1.2	11	3.7	0.5	0.37	0.94	0.09
139-857D-																													
3R-1, 117–120	0.34	70	0.5	45	290	680	3.6	15	86		38	110	230	36	3.9	230	110	12	6.4	3.8	1.1	6.0	1.4	12	4.1	0.6	0.48	0.78	0.55
4R-1, 138–140	1.91	30		47	160	1700	2	15	74		26	68	210	24	2.5	210	65	6.9	4.1	2.4	0.7	3.6	0.9	6.9	2.4	0.4	0.31	0.76	0.52
8R-1, 96–98	0.51	60	1	35	56	120	6.2	5	41		39	120	340	47	5.5	92	150	19	8.2	5.2	1.8	8.0	1.9	17	5.4	0.8	0.44	0.85	0.72
12R-1, 88–90	0.57	30		33	320	5	2.8	16	140		35	26	240	34	3.9	210	86	10	5.5	3.5	0.6	5.0	1.3	8.7	3.2	0.6	0.36	0.74	0.55
24R-1, 115–117	0.71	30	0.6	36	260	76	5.7	13	68		35	160	230	27	2.9	71	90	15	4.8	2.9	1.2	4.6	1.1	11	3.4	0.5	0.39	0.99	1.06
24R-2, 64–66	0.02	60	0.5	32	240	220	5.6	10	66		35	300	240	27	2.9	72	94	15	4.7	2.8	1.2	4.7	1.1	11	3.5	0.4	0.39	0.97	1.01
24R-2, 114–116	1.14	80	0.6	30	250	29	5.8	12	67		35	240	240	29	3.0	63	94	16	4.9	2.9	1.4	4.7	1.1	11	3.6	0.5	0.39	0.95	1.01
24R-3, 24–26	0.98	60	0.6	35	250	11	5.7	12	63		35	220	230	27	2.6	64	88	15	4.8	2.8	1.3	4.4	1.0	11	3.3	0.5	0.38	0.00	1.09
25R-1, 64–66	0.01	50	0.6	31	260	99	5.6	5	68		36	190	230	28	2.7	70	90	15	5.0	2.9	1.1	4.5	1.0	10	3.2	0.5	0.39	0.97	1.10
26R-1, 76–78	1.00	50	0.6	38	250	56	5.9	16	67		35	170	230	28	2.9	63	93	16	5.1	3.0	1.2	4.7	1.0	11	3.5	0.5	0.40	0.96	1.06
32R-1, 58–61	0.12	40	0.6	36	150	5	6.1	13	69		38	140	300	39	4.1	91	130	18	7.2	4.2	1.6	6.6	1.5	14	4.6	0.8	0.43	0.88	0.83
36R-1, 74–76	0.74	70	0.6	40	170	56	5.4	5	64		38	110	330	44	4.8	110	130	17	8.2	4.9	1.7	7.1	1.7	14	5.0	0.8	0.39	0.83	0.88
139-858F-																													
25R-1, 118–119	2.73	130	1.5	45	340	110	5.8	13	110	30	38	230	250	33	3.2	540	140	18	6.4	3.5	1.8	5.9	1.3	14	4.4	0.6	0.56	0.84	0.83
26R-1, 42–44	0.33	90	0.9	42	320	85	6.7	13	99		38	210	250	30	3.0	68	120	19	5.5	3.1	1.4	5.1	1.1	13	3.9	0.6	0.48	0.92	1.08
27R-1, 42–43	0.01	50	0.8	41	330	85	6.8	14	100		39	220	250	30	2.9	79	120	19	5.6	3.1	1.6	5.2	1.1	13	4.2	0.6	0.50	0.94	1.02
29R-1, 63–65	0.01	80	0.8	45	360	87	6.3	5	110		39	200	240	31	3.1	77	120	19	5.8	3.3	1.3	5.2	1.2	14	4.2	0.6	0.50	0.86	0.94
139-858G-																													
1R-1, 37–39	0.62	70	0.7	42	290	83	6.9	5	93		38	220	240	31	3.1	63	120	20	5.8	3.2	1.5	5.4	1.2	14	4.4	0.6	0.52	0.90	0.99
2R-1, 53–55	0.02	40	0.8	33	290	71	6.7	5	92		37	230	230	31	3.1	67	120	19	5.4	3.1	1.5	5.2	1.1	13	4.2	0.6	0.50	0.92	1.00
3R-1, 24–25	0.09	90	0.8	33	300	71	6.4	12	87		38	200	240	31	3.1	92	120	19	5.5	3.2	1.3	5.1	1.1	14	4.1	0.6	0.50	0.88	0.98
4R-1, 26–28	0.05	60	0.8	32	310	73	7.2	13	85		38	210	240	31	3.2	84	120	20	5.8	3.3	1.5	5.6	1.2	15	4.4	0.6	0.48	0.94	1.03
4R-1, 71–73	0.28	60	0.8	36	300	69	6.9	5	89		39	220	250	30	3.0	67	120	20	5.5	3.1	1.5	5.4	1.1	14	4.2	0.6	0.50	0.90	1.03
8R-1, 36–38	0.09	90	0.7	35	290	130	6.3	11	90		38	200	240	30	3.1	81	120	19	5.5	3.2	1.3	5.3	1.1	13	4.2	0.6	0.50	0.86	0.94
7R-1, 33–35	0.02	15	0.8	33	330	84	5.8	13	85	23	39	200	240	31	3.2	120	120	18	5.7	3.3	1.3	5.4	1.2	14	4.2	0.6	0.50	0.94	0.87
6R-1, 29–32	0.33	60	0.8	33	300	85	6.5	11	89	28	38	220	240	30	3.2	150	120	19	5.6	3.3	1.3	5.2	1.1	14	4.3	0.6	0.48	0.89	0.95
5R-1, 16–18	1.28	70	0.7	40	330	56	6.8	15	93	43	40	220	250	29	2.9	150	120	20	5.6	3.1	1.5	5.2	1.1	14	4.1	0.6	0.52	0.89	1.04
10R-1, 31–33	1.13	80	0.8	39	290	60	6.3	15	85		37	210	230	30	3.0	83	120	19	5.4	3.1	1.4	5.0	1.1	14	4.1	0.5	0.48	0.86	0.97
10R-1, 104–106	0.70	70	0.7	43	300	190	7	10	90		39	220	250	31	3.0	67	120	20	5.9	3.3	1.4	5.3	1.2	15	4.4	0.6	0.48	0.91	1.00
11R-1, 13–15	0.02	60	0.8	36	300	76	6.2	11	85		39	210	250	31	3.3	69	120	18	5.7	3.3	1.4	5.2	1.2	14	4.2	0.6	0.50	0.90	0.93
12R-1, 48–50	2.02	60	0.8	44	300	49	6.4	12	94		39	220	240	30	3.0	63	120	18	5.4	3.2	1.7	5.0	1.1	13	3.8	0.5	0.50	0.93	1.06
13R-1, 9–11	0.16	80	0.7	41	280	260	6.5	5	98		36	220	240	31	3.1	84	120	19	5.5	3.2	1.4	5.1	1.1	13	4.0	0.5	0.48	0.89	1.02
13R-1, 25–27	0.76	40	0.8	46	310	95	6.5	5	94		39	220	250	31	3.0	71	120	19	5.3	3.2	1.5	5.2	1.1	13	3.8	0.5	0.48	0.89	1.08
14R-1, 41–43	0.04	60	0.7	35	310	100	6.2	5	91		40	220	250	30	3.0	71	120	18	5.6	3.2	1.4	5.2	1.1	13	3.9	0.5	0.46	0.90	1.00
15R-1, 31–33	0.78	50	0.8	52	300	170	6.6	14	99		41	210	260	31	3.1	74	130	20	6.0	3.4	1.5	5.6	1.2	14	4.2	0.6	0.52	0.86	0.99
16R-1, 77–79	1.29	60	0.7	43	340	55	6.3	10	84		40	220	250	29	2.8	95	130	19	5.3	3.1	1.5	5.2	1.1	13	4.1	0.5	0.00	0.86	0.97

Notes: For $[La/Ce]_n$ and $[La/Sm]_n$, n signifies that values are normalized to chondritic values. Analyses of trace elements by ICP-ES. Analyses of Y and REE by ICP-MS.

mid-ocean ridge basalt (N-MORB) based on Zr/Nb, $[La/Sm]_n$ (Le Roex et al., 1983; Karsten et al., 1990; Michael et al., 1989) or $[La/Ce]_n$ (Langmuir et al., 1977; Basaltic Volcanism Study Group, 1981; Van Wagoner and Leybourne, 1991). We are using the classifications adopted by Karsten et al. (1990) for Zr/Nb and Van Wagoner and Leybourne (1991) for [La/Ce]n. The low Nb content in these samples renders the Zr/Nb values of questionable value. These will be referred to based on shipboard Nb values, but basalt classification

Table 2. Oxygen isotopic compositions of whole rock powders.

Core, section, interval (cm)	Depth (mbsf)	O^{18}
139-855A-		
8R-1, 26–28	65.1	7.2
9R-1, 37–39	74.7	7.6
9R-1, 26–28	74.6	8.0
139-855D-		
5R-1, 29–31	108.8	7.0
139-856A-		
13X-CC, 11–16	113.3	6.5
14X-CC, 3–7	115.8	7.1
14X-1, 56–61	115.1	6.5
139-856B-		
9X-1, 4–8	62.3	9.2
139-857C-		
59R-1, 106–108	472.2	5.5
59R-2, 138–139	474.0	5.3
59R-3, 101–103	475.0	5.2
60R-1, 13–15	480.9	4.9
62R-1, 46–48	500.5	4.6
62R-2, 60–62	502.1	4.5
64R-1, 63–66	520.0	4.8
64R-2, 33–35	521.2	4.6
65R-1, 15–17	529.3	7.5
66R-1, 15–17	539.0	6.8
66R-1, 25–27	539.1	2.9
66R-1, 114–116	539.9	4.5
67R-1, 55–57	549.0	6.6
68R-1, 26–29	558.3	3.2
68R-1, 108–111	559.1	4.7
68R-2, 11–13	559.6	4.2
68R-2, 144–146	560.9	4.6
139-857D-		
1R-1, 2–4	581.5	4.2
1R-2, 82–84	583.8	4.0
2R-1, 73–75	590.3	4.7
2R-1, 77–79	590.4	4.4
3R-2, 67–69	601.4	4.3
3R-2, 94–96	601.7	4.2
4R-1, 9–11	609.0	4.3
7R-1, 16–18	637.8	4.5
4R-1, 88–90	609.8	4.3
8R-1, 73–75	648.0	2.4
15R-1, 58–60	715.4	3.3
18R-1, 55–58	744.2	4.5
18R-1, 98–101	744.6	4.3
18R-2, 84–87	745.9	4.6
20R-1, 64–67	763.1	4.3
21R-1, 62–65	772.8	4.5
22R-1, 52–55	782.3	4.1
23R-1, 80–84	792.3	4.3
24R-1, 112–115	802.3	4.9
24R-2, 100–103	803.7	4.5
26R-1, 16–19	820.5	4.7
27R-1, 96–98	830.6	4.7
29R-1, 145–148	849.9	4.6
31R-1, 68–70	869.2	4.8
32R-1, 60–65	878.7	5.1
33R-1, 75–79	888.6	4.3
35R-1, 27–29	907.5	4.2
36R-1, 13–15	917.0	4.3
36R-1, 67–69	917.6	4.6
139-858F-		
25R-1, 111–113	250.0	4.5
26R-1, 63–65	259.2	5.2
26R-1, 98–100	259.6	5.1
27R-1, 39–41	268.2	5.4
28R-1, 30–32	277.8	5.0
29R-1, 9–11	287.3	5.4
29R-1, 81–83	288.0	4.9
9R-CC, 18–20	94.4	7.1
25R-1, 40–42	249.3	6.2
25R-1, 118–119	258.1	4.2
26R-1, 42–44	259.0	5.4
27R-1, 42–43	268.2	5.4
29R-1, 65–67	287.9	4.9
139-858G-		
1R-1, 37–39	277.2	4.9
2R-1, 53–55	287.0	5.3
3R-1, 24–25	296.3	4.8
4R-1, 26–28	306.1	5.1
4R-1, 71–73	306.5	5.5
5R-1, 16–18	315.6	5.8
6R-1, 29–32	325.4	5.1
7R-1, 33–35	335.1	4.8
8R-1, 36–38	344.9	4.5
10R-, 31–33	365.2	4.9
10R-1, 104–106	366.0	4.6
11R-1, 16–18	374.5	5.6
12R-1, 48–50	384.7	5.0
13R-1, 9–11	394.0	5.0
13R-1, 25–27	394.2	4.7
14R-1, 41–43	404.0	5.2
15R-1, 31–33	413.6	4.9
16R-1, 77–79	423.7	5.1

is determined by the more reliable $[La/Ce]_n$. The values for Zr/Nb (22–40; Davis, Mottl, Fisher, et al., 1992) categorizes these as T-MORBs (= 16 < Zr/Nb < 25) and N-MORBS (Zr/Nb >25). The more reliable REE (below) categorize these as all N-MORBs. The data form a linear array in a plot of Zr vs. Ti (Fig. 3A).

The REE patterns (Fig. 4B) are typical of N-type MORB derived from depleted mantle in that they are light REE depleted and otherwise flat to slightly HREE-depleted (Fig. 4). Values for chondrite-normalized La/Sm ($[La/Sm]_n = 0.54–0.66$); La/Ce ($[La/Ce]_n = 0.76–0.82$) and Ce/Yb ($[Ce/Yb]_n = 0.76–0.89$) confirm the depleted nature of their mantle source region (Fig. 3, Table 1, section B). A pronounced negative europium anomaly is evident in the most fractionated (highest REEs) sample, probably resulting from fractionation of plagioclase.

Site 856, Holes A and B

Setting

At Site 856, a series of drillholes was located across a topographic high referred to as "Bent Hill," which is about 60 m high and about 500 m in diameter. In Holes 856G and 856H, 65 m and 95 m of massive sulfide, respectively, were cored. Small quantities of mafic igneous rock were drilled at the bottom of Holes 856A and 856B and from a 5–8-m-thick sill that was drilled through completely in Hole 856B (Davis, Mottl, Fisher, et al., 1992). All the samples are inferred to be from sills based on the nature of the chilled contacts and rapid increase in grain size from the margins (Davis, Mottl, Fisher, et al., 1992). The margins of the sills have thin glassy rims which are typically replaced by chlorite and quartz. Some of the contacts are evidenced only by small fragments of bleached basalt with coatings of baked sediment. Most of the igneous rocks recovered, however, are holocrystalline with a microcrystalline to fine-grained groundmass of variolitic plagioclase and clinopyroxene. The mesostasis in a few samples is replaced by small quantities of greenschist-grade minerals including chlorite, epidote, and actinolite.

Table 3. Microprobe analyses of olivine phenocryst compositions, Leg 139, Sites 855 and 856.

	1[a]	2b	3[c]	4[d]	5[e]	6[f]	7[g]
SiO_2	38.88	38.26	39.76	40.31	39.81	40.83	40.73
Al_2O_3	0.08	0.01	0.03	0.04	0.08	0.06	0.07
Cr_2O_3	0.00	0.01	0.01	0.03	0.06	0.04	0.06
MgO	43.72	39.26	44.57	48.23	46.61	48.89	48.56
CaO	0.33	0.29	0.33	0.29	0.36	0.28	0.33
MnO	0.22	0.36	0.25	0.19	0.15	0.13	0.19
FeO	16.26	21.13	15.37	10.90	12.46	10.43	10.03
Total	99.50	99.33	100.32	99.99	99.53	100.65	99.95
Si	0.992	0.998	0.998	0.994	0.994	0.997	1.000
Al	0.002	0.000	0.001	0.001	0.002	0.002	0.002
Cr	0.000	0.000	0.000	0.001	0.001	0.001	0.001
Mg	1.674	1.526	1.667	1.773	1.734	1.780	1.777
Ca	0.009	0.008	0.009	0.008	0.010	0.007	0.009
Mn	0.005	0.008	0.005	0.004	0.003	0.003	0.004
Fe	0.349	0.461	0.323	0.225	0.260	0.213	0.206
Catsum	3.032	3.002	3.002	3.005	3.005	3.002	2.998
Fo	82.74	76.81	83.93	88.91	87.25	89.53	89.83
Fa	17.26	23.19	16.24	11.27	13.09	10.71	10.41

[a] 139-855A-8R-1, 21–23 cm, large euhedral grain.
[b] 139-855A-8R-1, 35–37 cm, rim of zoned olivine.
[c] 139-855D-5R-1, 15–17 cm, core of large grain.
[d] 139-856A-14X-1, 23–26 cm, core of large grain.
[e] 139-856A-14X-1, 23–26 cm, rim of same large grain as previous.
[f] 139-856A-14X-1, 85–87 cm, core of large grain.
[g] 139-856B-8H-CC, 1–3 cm, core of large grain.

Petrography and Mineral Chemistry

Olivine is present as phenocrysts in all samples, both as large subhedral crystals and small rounded crystals. The large crystals tend to be broken and replaced along fractures, or to contain groundmass minerals along fractures. The olivine crystals are highly magnesian ($Fo_{88–90}$; Table 3) and are typically unzoned. They frequently occur in megacrystic aggregates with euhedral spinel, an association characteristic of crystal accumulates. The olivine phenocrysts comprise 2%–8% of the rock.

Spinel is present as brownish-red to deep red euhedral crystals that are associated with the large olivines and commonly occur as inclusions within the olivines. The spinels rarely contain inclusions of smectite or chlorite, presumably as replacements of glass. The spinels are highly magnesian (Table 6) and are typically unzoned. A few crystals do have a Cr-rich rim, however, which is also conspicuous by having a deeper color. The Mg numbers of the spinels vary from 0.5 to 0.9 and the Cr numbers vary from 0.3 to 0.5 (Figs. 5A, 5B).

In addition to the Cr-Mg-Al spinels, the principal oxide phase is titanomagnetite (Table 7, section A). These grains are generally intersertal to plagioclase and ferromagnesian grains and are typically about 0.5 mm in width. In some areas titanomagnetite forms distinct rims on the Cr-rich spinels, indicating that it formed slightly later than spinel. Isolated grains of titanomagnetite have an average composition of $(Fe^{3+}0.78\ Fe^{2+}1.51\ Ti_{0.56}\ V_{0.03}\ Mn_{0.05})\ O_4$. They are not altered, and appear to be unzoned. Where titanomagnetite either rims or is intergrown with spinel it has a higher Cr content than those grains that formed independently of spinel. In Sample 139-856A-14X, 90–92 cm, for example, titanomagnetite surrounding spinel contains 9.5 weight percent (wt%) Cr_2O_3 and 2.98 (wt%) V_2O_5.

Table 4. Plagioclase compositions, Leg 139, Sites 855-858, representative analyses of fresh and unaltered phases.

	1[a]	2[b]	3[c]	4[d]	5[e]	6[f]	7[g]	8[h]	9[i]	10[j]	11[k]	12[l]	13[m]	14[n]	15[o]	16[p]	17[q]	18[r]
SiO_2	46.25	47.63	50.31	49.70	51.65	50.26	51.42	51.23	52.34	54.57	55.97	46.00	49.14	51.41	56.68	51.99	55.49	67.81
Al_2O_3	34.31	32.99	32.60	32.06	29.81	32.10	30.85	31.24	29.36	29.16	28.07	34.85	32.64	30.64	26.18	30.20	27.86	21.05
Fe_2O_3*	0.53	0.41	0.58	0.65	1.01	0.46	0.67	0.48	0.97	0.87	1.15	0.41	0.69	0.75	0.98	0.73	1.19	0.03
CaO	17.57	16.07	15.79	15.59	13.27	15.09	14.02	14.92	14.00	11.96	10.64	18.62	15.92	13.23	9.07	13.16	10.47	1.41
Na_2O	1.61	2.17	2.50	2.58	3.50	2.69	3.27	2.98	3.48	4.36	5.12	1.04	2.36	3.63	6.08	3.58	5.07	9.63
K_2O	0.00	0.02	0.03	0.00	0.01	0.00	0.01	0.02	0.03	0.06	0.06	0.00	0.01	0.04	0.12	0.03	0.08	0.09
Total	100.27	99.29	101.80	100.59	99.25	100.61	100.23	100.86	100.18	100.98	101.01	100.92	100.76	99.70	99.10	99.67	100.14	100.01
Si	2.125	2.194	2.258	2.259	2.348	2.277	2.333	2.314	2.378	2.442	2.498	2.105	2.232	2.338	2.570	2.366	2.498	2.952
Al	1.858	1.791	1.724	1.717	1.597	1.714	1.650	1.663	1.572	1.538	1.477	1.877	1.748	1.643	1.399	1.620	1.478	1.080
Fe	0.018	0.016	0.019	0.022	0.038	0.016	0.023	0.016	0.033	0.029	0.039	0.014	0.024	0.029	0.033	0.025	0.040	0.001
Ca	0.865	0.793	0.759	0.759	0.646	0.733	0.681	0.722	0.682	0.574	0.509	0.912	0.775	0.645	0.441	0.642	0.505	0.066
Na	0.144	0.194	0.218	0.227	0.309	0.236	0.288	0.261	0.307	0.378	0.443	0.092	0.208	0.320	0.534	0.316	0.442	0.813
K	0.000	0.001	0.002	0.000	0.001	0.000	0.000	0.001	0.002	0.004	0.004	0.000	0.001	0.003	0.007	0.002	0.004	0.005
Catsum	5.009	4.989	4.980	4.985	4.938	4.976	4.975	4.977	4.974	4.965	4.968	5.000	4.987	4.976	4.984	4.970	4.967	4.916
Ab	14.3	19.63	22.26	23.02	32.30	24.38	29.68	73.40	68.84	39.57	46.36	9.15	21.13	33.08	54.42	32.91	46.48	92.03
An	85.7	80.35	77.56	76.95	67.64	75.61	70.28	26.50	30.98	60.05	53.27	90.84	78.79	66.66	44.90	66.92	53.06	7.42
Or	0.00	0.12	0.18	0.02	0.06	0.01	0.04	0.10	0.18	0.38	0.36	0.01	0.08	0.26	0.69	0.17	0.46	0.55

Note: Fe_2O_3* = total Fe expressed as Fe_2O_3.

[a] 139-855A-8R-1, 21–23, 2 cm, core of zoned plagioclase.
[b] 139-855A-8R-1, 18–19, 2 cm, small phenocryst intergrown with pryroxene.
[c] 139-855A-8R-1, 18–19, 2 cm, small phenocrysts intergrown with Cr-rich pyroxene.
[d] 139-855-5R1, 15–17 cm, core, large phenocryst.
[e] 139-855-5R-1, 15–17 cm, rim, large phenocryst.
[f] 139-856B-10H, 74–77 cm, rim of thin microphenocryst.
[g] 139-856B-10H, 74–77 cm, skeletal plagioclase.
[h] 139-856A-14X-CC, 20–22 cm, core of euphedral lath.
[i] 139-856A-14X-CC, 20–22 cm, rim of euhedral lath.
[j] 139-857D-17R-3, 89–91 cm, rim of altered grain.
[k] 139-857D-17R-3, 89–91 cm, rim of altered grain.
[l] 139-857D-12R-1, 51–53 cm, core of xenocryst.
[m] 139-857D-12R-1, 51–53 cm, small euhedral phenocryst.
[n] 139-857C-59R-1, 145–147 cm, grain poikilitically intergrown with pyroxene.
[o] 139-857C-59R-1, 145–147 cm, rim of altered grain.
[p] 139-858-G-1R-1, 27–29 cm, core of thin lath.
[q] 139-858G-1R-1, 27–29 cm, rim of thin lath.
[r] 139-858G-16R-1, 47–49 cm, altered patch in phenocryst.

All of the rocks contain plagioclase both as a groundmass phase and as phenocrysts. There is a continuous gradient in the size of the plagioclase crystals from large subhedral or embayed crystals to small lathlike crystals intergrown with clinopyroxene. The plagioclase is rarely replaced by pale aluminous epidote, but is more typically fresh. Most plagioclase is moderately calcic (An_{74-79}) but more sodic compositions are found as groundmass phases or rims on larger crystals (An_{64-70}).

Clinopyroxene is never observed as a phenocryst phase in these samples as was observed at Site 855. It is present only in the groundmass in variolitic bundles or small needle-like aggregates.

Sulfides in the least-altered samples examined (139-856A-14X-1, 7–9 cm, 86–88 cm, 90–92 cm) occur as polysulfide aggregates. These aggregates occur primarily as inclusions in plagioclase phenocrysts, but also occur as irregular to spherical blebs in the mesostasis. The latter resemble classic "immiscible sulfide" droplets common to all magmatic sulfide bodies. The inclusions and bleb aggregates are usually about 50 microns in diameter. The sulfide aggregates are composed primarily of pyrrhotite, with exsolved lamellae and blebs of pentlandite and minor chalcopyrite. Microprobe analyses of these sulfides (Table 8) indicate that the pyrrhotite is nickel-rich. Analyses of one such bleb in Sample 139-856A-14x-1, 90–92 cm illustrates that the exsolution of pentlandite is not complete, as the adjacent pyrrhotite has nickel contents varying from 1.08% to 4.84%. The most Ni-rich pyrrhotite contains 3.64% copper, indicating incomplete subsolidus exsolution of copper as well as nickel from this portion of the sulfide bleb. The most Fe-rich pentlandite corresponds to the most Ni-rich pyrrhotite, indicating that the system has remained closed with respect to sulfur. This suggests that seawater did not penetrate into the center of these thin intrusions as would be anticipated with hydrothermal cooling of the sills. Equilibrium exsolution was not reached, as is indicated by the highly variable amount of Ni and Cu in the probe data. As these intrusions were emplaced close to the seafloor (ca. 115 mbsf), heat loss from them was rapid and complete exsolution of pentlandite and copper minerals was prevented. The most-altered samples from this site (Samples 139-856B-10H-1, 93–95 cm and 10H-2, 2–9 cm; see discussion of petrochemical data, below) come from the shallowest of these intrusions. Here, only pyrite is present, as subhedral to euhedral grains. Its nickel contents are comparable with those of the primary pyrrhotite and much higher than the nickel contents of hydrothermal pyrite (Franklin et al., unpubl. data).

Major Element Composition

The new data provided as part of this study confirm the shipboard observations (Davis, Mottl, Fisher, et al., 1992) that these rocks are similar to the most primitive rocks of the northern Juan de Fuca, the olivine-phyric flows of West Ridge (Van Wagoner and Leybourne, 1991). All of these intrusions have been hydrated, and all may have been somewhat altered. However, the silicate phenocrysts are predominantly fresh and oxide and sulfide phases appear very fresh. An exception is Sample 139-856B-10H-1, 93–95 cm, from the margin of the sill drilled through in Hole 856A, which is highly altered. It contains an unusually high potash content, high titania and alumina, all characteristics of the extremely leached basalt-sediment chilled contacts observed in Site 856 and Site 857. This sample has been eliminated from the subsequent plots. In the fresh samples, the SiO_2, TiO_2, FeOT and P_2O_5 contents are all lower than in the samples from the other sites (Table 1; Fig. 2), due in part to dilution by olivine megacrysts. However, samples from Site 856 are slightly more aluminous and have much higher Mg numbers than samples from the other sites. Their Mg# is 73, distinctly higher than that for samples from the Southern Juan de Fuca, Endeavour (Karsten et al., 1990), Heck and Heckle seamounts (Leybourne and Van Wagoner, 1991), West Valley (Van Wagoner and Leybourne, 1991), or Explorer Ridge

Table 5. Microprobe analyses of clinopyroxene compositions, Leg 139, Sites 855, 857, and 858.

	1[a]	2[b]	3[c]	4[d]	5[e]	6[f]	7[g]	8[h]	9[i]	10[j]	11[k]	12[l]	13[m]	14[n]
SiO_2	50.480	49.830	50.020	51.530	52.180	50.080	51.800	45.730	50.940	51.100	50.530	50.420	52.700	50.37
TiO_2	0.500	1.230	1.100	0.990	0.660	1.150	0.680	3.540	0.850	1.100	1.200	1.280	0.580	1.21
Al_2O_3	3.960	4.150	4.190	3.900	2.650	4.600	3.950	6.090	1.860	3.280	2.780	3.900	1.810	1.83
Fe_2O_3	2.216	1.869	1.939	0.627	1.115	1.397	0.451	2.274	0.625	1.000	1.817	1.443	0.000	1.19
FeO	2.886	5.918	5.826	5.426	4.927	4.593	4.704	9.904	13.268	8.190	9.205	6.752	7.620	14.13
MnO	0.240	0.190	0.170	0.150	0.230	0.130	0.180	0.220	0.440	0.250	0.290	0.200	0.280	0.41
MgO	17.020	16.070	16.500	17.310	17.640	16.710	16.830	10.880	13.100	15.910	15.260	15.520	16.770	12.55
CaO	20.370	19.270	18.810	19.090	19.730	19.530	20.440	20.570	18.200	18.240	18.240	19.890	18.970	18.00
Na_2O	0.270	0.270	0.280	0.350	0.240	0.300	0.320	0.430	0.280	0.280	0.310	0.290	0.210	0.29
Cr_2O_3	1.430	0.590	0.740	0.240	0.220	0.920	1.520	0.100	0.000	0.160	0.070	0.360	0.410	0.00
Sum	99.372	99.387	99.575	99.613	99.592	99.410	100.875	99.738	99.563	99.510	99.702	100.055	99.350	99.98
Si	1.858	1.850	1.850	1.889	1.914	1.846	1.880	1.743	1.935	1.892	1.890	1.864	1.951	1.918
Ti	0.014	0.034	0.031	0.027	0.018	0.032	0.019	0.101	0.014	0.031	0.034	0.036	0.016	0.035
Al	0.172	0.182	0.183	0.169	0.115	0.200	0.169	0.274	0.083	0.143	0.123	0.170	0.079	0.082
Fe_3	0.061	0.052	0.054	0.017	0.031	0.039	0.012	0.065	0.018	0.028	0.051	0.040	0.000	0.034
Fe_2	0.089	0.184	0.180	0.166	0.151	0.142	0.143	0.316	0.422	0.254	0.288	0.209	0.236	0.450
Mn	0.007	0.006	0.005	0.005	0.007	0.004	0.006	0.007	0.104	0.008	0.009	0.006	0.009	0.013
Mg	0.934	0.889	0.910	0.946	0.965	0.918	0.910	0.618	0.742	0.878	0.850	0.855	0.925	0.712
Ca	0.804	0.766	0.746	0.750	0.776	0.771	0.795	0.840	0.741	0.743	0.731	0.788	0.752	0.734
Na	0.019	0.019	0.020	0.025	0.017	0.021	0.023	0.032	0.021	0.020	0.022	0.021	0.015	0.021
Cr	0.042	0.017	0.022	0.007	0.006	0.027	0.044	0.003	0.000	0.005	0.002	0.011	0.012	0.000
Catsum	4.000	3.999	4.001	4.001	4.000	4.000	4.001	3.999	4.080	4.002	4.000	4.000	3.995	3.999
Wo	44.00	41.67	40.62	40.27	41.01	42.13	43.10	47.36	38.91	89.64	39.10	42.55	39.32	38.72
En	51.53	48.34	49.56	50.79	51.00	50.14	49.26	34.84	38.95	46.83	45.50	46.18	48.35	37.55
Fs	4.87	9.99	9.82	8.93	7.99	7.73	7.73	17.80	22.14	13.53	15.40	11.27	12.33	23.73

[a] 139-855A-8R-1, 21–23 cm, megacryst in glass host.
[b] 139-855A-8R-1, 18–19 cm, core of pyroxene phenocryst.
[c] 139-855A-8R-1, 18–19 cm, rim of zoned phenocrysts.
[d] 139-857C-59R-1, 16–18 cm, phenocryst.
[e] 139-857C-60R-2, 17–19 cm, core of reversely zoned pyroxene.
[f] 139-857C-60R-2, 17–19 cm, rim of reversely zoned pyroxene.
[g] 139-857C-59R-3, 140–142 cm, cr-rich core of pyroxene.
[h] 139-857C-66R-1, 108–110 cm, rim of brownish pyroxene.
[i] 139-857D-17R-3, 89–91 cm, core of anhedral pyroxene.
[j] 139-857D-17R-3, 89–91 cm, rimof anhedral pyroxene.
[k] 139-857D-35R-1, 87–90 cm, small barrel-shaped crystal.
[l] 139-857D-35R-1, 87–90 cm, rim of zoned pyroxene.
[m] 139-857D-35R-1, 87–90 cm, poikilitic intergrowth.
[n] 139-857D-35R-1, 87–90 cm, poikilitic intergrowth.

(Cousens et al., 1984) areas. The Mg# calculated on the basis on the whole-rock chemistry is biased by the accumulation of phenocrysts compared to the chemistry of the original fresh glass. The Mg# based on the chromian spinel compositions (see Discussion), however, is not biased in this way and still distinguishes these magmas as extreme compositions, although similar to the most primitive compositions from West Ridge, West Valley South or the Heck Seamounts.

Minor and Trace Element Composition

These samples are more chromian and nickel rich than other mafic rocks in the Middle Valley area, reflecting the abundant spinel and primary sulfide accumulations noted above. The sulfur content of the samples from Site 856 are reasonably uniform (330 to 1400 ppm). Nickel, copper, and zinc are within the range of normal basaltic melts with averages of 220, 77, and 68 ppm, respectively. The sulfur content of the samples (1400 ppm maximum) is only slightly higher than that predicted for sulfur-saturated melts of composition similar to Site 856 samples (Mathez, 1980), indicating that sulfur has not been added during alteration. Furthermore, the MgO contents of the unaltered samples correlate well with their Ni contents, i.e., with modal olivine. Had Mg been added from seawater through alteration, this correlation would be nonexistent. The replacement of olivine by talc and magnetite appears to be a static hydration not associated with substantial change in chemistry. The replacement of oxides (e.g., spinel) by sulfide was only observed in the narrow, highly-altered contact zone with sediments.

The Site 856 samples contain lower contents of most of the incompatible elements than the other sites, partially due to dilution by crystal accumulation (Figs. 3 and 4). All of the samples are homogeneous, forming tight clusters on most of the plots. On the Zr vs. TiO_2 plot, they fall at the low Zr and low TiO_2 end of the plot, similar to primitive basalts, and form a linear array distinct from the other sites. Their Zr/Nb values (22–50) (Davis, Mottl, Fisher, et al., 1992) classify them as T-MORB to N-MORB but the low values of Nb make this classification unreliable. Values for $[La/Sm]_n$ (0.28–0.29), $[La/Ce]_n$ (0.65–0.70) and $[Ce/Yb]_n$ (0.37–0.39) are significantly lower than those for Site 855 (Fig. 3) and classify them more reliably as N-MORB. The only exception is the slightly altered Sample 139-856B-10H-1R, 64–67 cm, which has values falling between those of the adjacent, highly altered sample and the remaining analyses. Thus, the contact alteration may have produced a spuriously high $[La/Ce]_n$ value (or may have mixed in some sediment, M. Leybourne, pers. comm., 1993). Their chondrite-normalized REE patterns indicate that they are quite homogeneous and typified by LREE depletion and flat HREE (Fig. 4). The REE patterns are similar to those for the Heck and Heckle seamounts to the west of Middle Valley and Endeavour Ridge (Leybourne and Van Wagoner, 1991) and the depleted magmas of West Ridge (Van Wagoner and Leybourne, 1991), but are quite distinct from LREE-enriched patterns for samples from Endeavour Ridge (Karsten et al., 1990) or West Valley (Van Wagoner and Leybourne, 1991).

Site 857, Holes C and D

Setting

Sites 857 and 858 are located 6 km west of the eastern boundary fault and 6 km west of the Middle Valley spreading axis (Fig. 1). The sites are 1.6 km apart along a north-south line and lie within a 15-km-long thermal anomaly that parallels the rift within which heat flow exceeds 0.8 Wm^{-2} (Davis, Mottl, Fisher, et al., 1992). Igneous rock recovered at Site 857 is from a series of variably metamorphosed 1- to

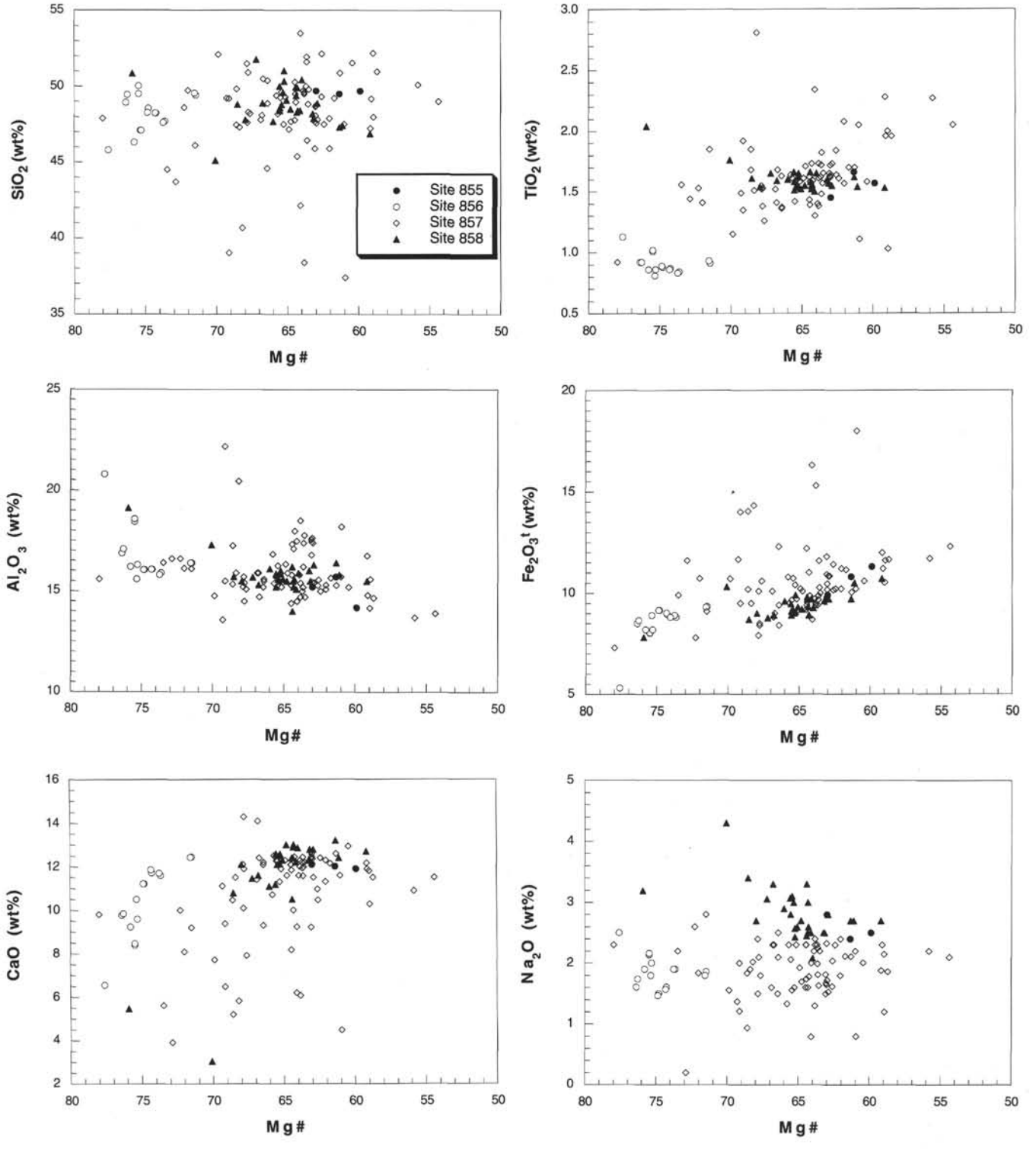

Figure 2. Major element chemistry for all sites, Leg 139.

25-m-thick mafic sills interlayered with altered and indurated sediment. For many of the intrusive units, a fine-grained chilled margin and coarse-grained interior could be readily identified in the drillcore. This, combined with the resistivity data collected by shipboard logging, indicates relatively complete sampling across individual sills. The interiors of the larger sills are extremely coarse grained and composed of poikilitically intergrown plagioclase and clinopyroxene with ilmenite or magnetite and fine-grained mesostasis. Extreme variability of texture and crystal size is a conspicuous characteristic of the sills and results from variations in cooling rate from the sill margins to the interiors. This variability is mirrored in clinopyroxene compositions described below. Comparison between the intervals of recovered igneous rock and levels of high resistivity logged in Hole 857C suggest recovery modestly estimated at over 50%. Similar compari-

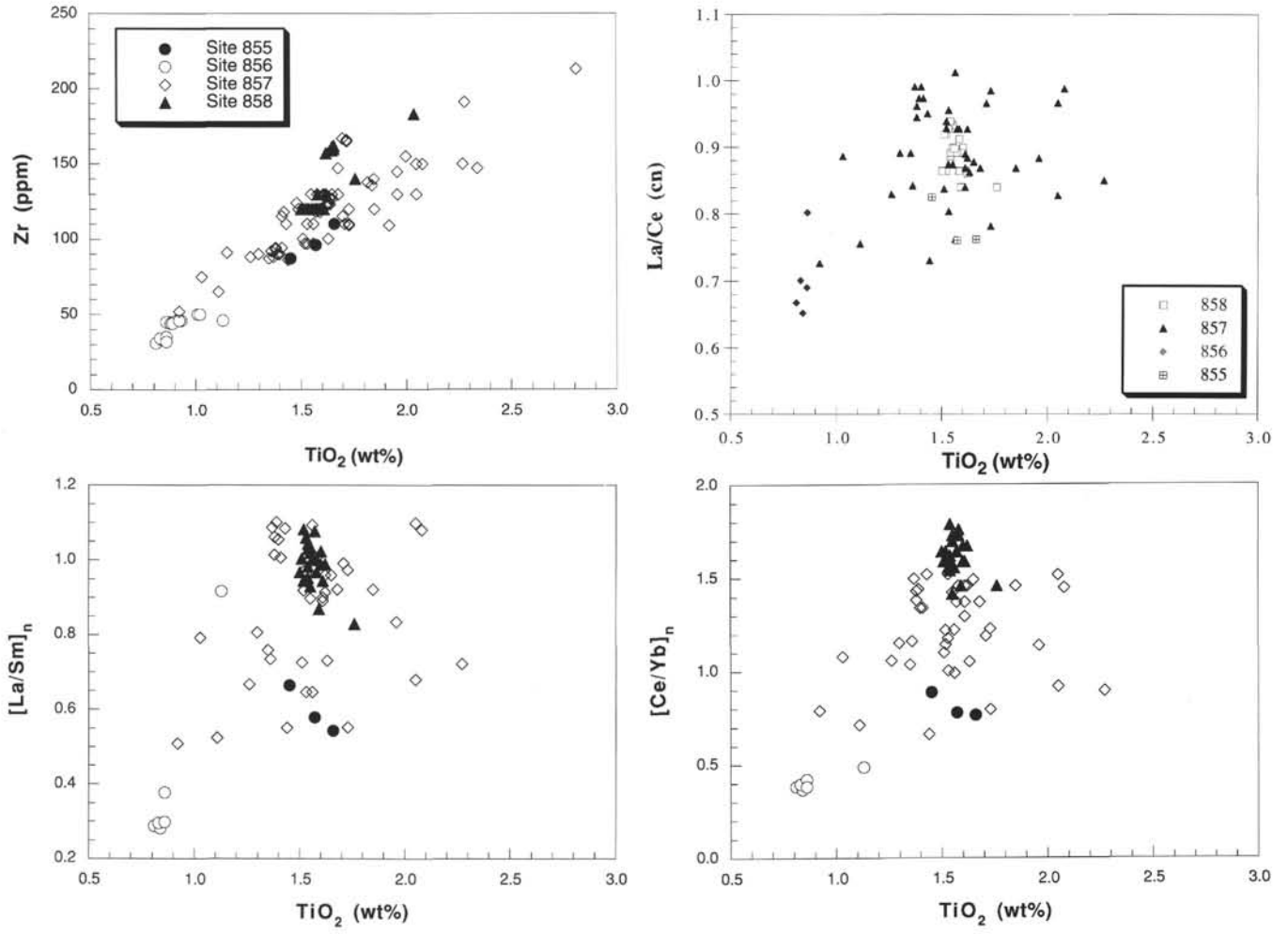

Figure 3. Trace element chemistry for all sites, Leg 139.

sons for Hole 857D suggests a slightly lower, but still high recovery of the igneous units (Davis, Mottl, Fisher, et al., 1992).

Site 857 Lithostratigraphy

Both Holes 857C and 857D were logged, and the resistivity log proved useful in discriminating sills vs. sediments (Davis, Mottl, Fisher, et al., 1992, pp. 364–365). The log from Hole 857D (which includes most of the sill horizon from Hole 857C) suggested that there were 32 distinct sills between 465 and 934 mbsf for a combined thickness of 165 m of igneous rock. Detailed lithostratigraphy from Davis, Mottl, Fisher, et al. (1992) is expanded here with new mineral data and is summarized in Table 9. Igneous rock was first encountered in Core 857C-59R (Unit 1), the top of which is fine-grained diabase with plagioclase and pyroxene phenocrysts and megacrysts that increase in size and compositional zoning (plagioclase = An_{56-73}) with depth. In Sections 139-857C-59R-2 and 857C-59R-3 the ophitic texture is extremely coarse-grained (plagioclase = An_{52-67}). The texture systematically decreases in grain size and changes in Section 857C-59R-4 to sub-ophitic or diabase, although no chill or sediments were observed in this core. The top of Core 139-857C-60R (Unit 2) contains a chilled margin of fine-grained basalt with plagioclase phenocrysts whose texture coarsens conspicuously in the lower half of Section 857C-60R-1 to a medium-grained diabase with strongly zoned plagioclase. The upper 20 cm of Section 857C-60R-2 is a diabase with zoned plagioclase phenocrysts (An_{53-66}) that systematically decreases in grain size to a well-preserved basal contact with sediment. Diabase is again present at 857C-60R-2, 49–142 cm (Unit 3), mostly as small unoriented pieces, including some coarse-grained samples. Phyric diabase with zoned plagioclase and pyroxene continues to Section 857C-61R-1, 100 cm (Unit 4), where there is a sharp contact with sediment. The rock at the contact is fine-grained with plagioclase microlites and phenocrysts. The top of Section 857C-61R-2 is a fine-grained contact to a phyric diabase which makes up the remainder of Core 857C-61R (Unit 5). Core 857C-62R is composed of medium to coarse-grained diabase or ophite with pyroxene enclosing plagioclase (An_{51}) in a poikilitic texture and macroscopically conspicuous laths of ilmenite and granular magnetite. The coarsest grain size (e.g., 139-857C-62R-2, 12–14 cm) has large euhedral ilmenites extensively altered to leucoxene and strongly zoned plagioclase (An_{50-70}) and clinopyroxene (brown titaniferous rims). There is increased alteration at this horizon with clinopyroxene partially replaced by actinolite and islands of sodic plagioclase in large patches of chlorite. There are no contacts with sediment and no apparent reduction in grain size (Unit 6). The top of Core 857C-63R, however, is metamorphosed sediment with a diabase contact within a gravel horizon composed of mixed sediment and vesicular igneous fragments. The remainder of Core 857C-63R is a coarse-grained diabase with strongly zoned plagioclase (An_{32-70}) and zoned poikilitic pyroxene with ilmenite laths (Unit 7). Core 857C-64R is similarly coarse-grained diabase with subophitic texture and poikilitic clinopyroxene and skeletal ilmenite (Unit 8). A slight decrease in grain size occurs at the bottom of Section 857C-64R-2, where fine-

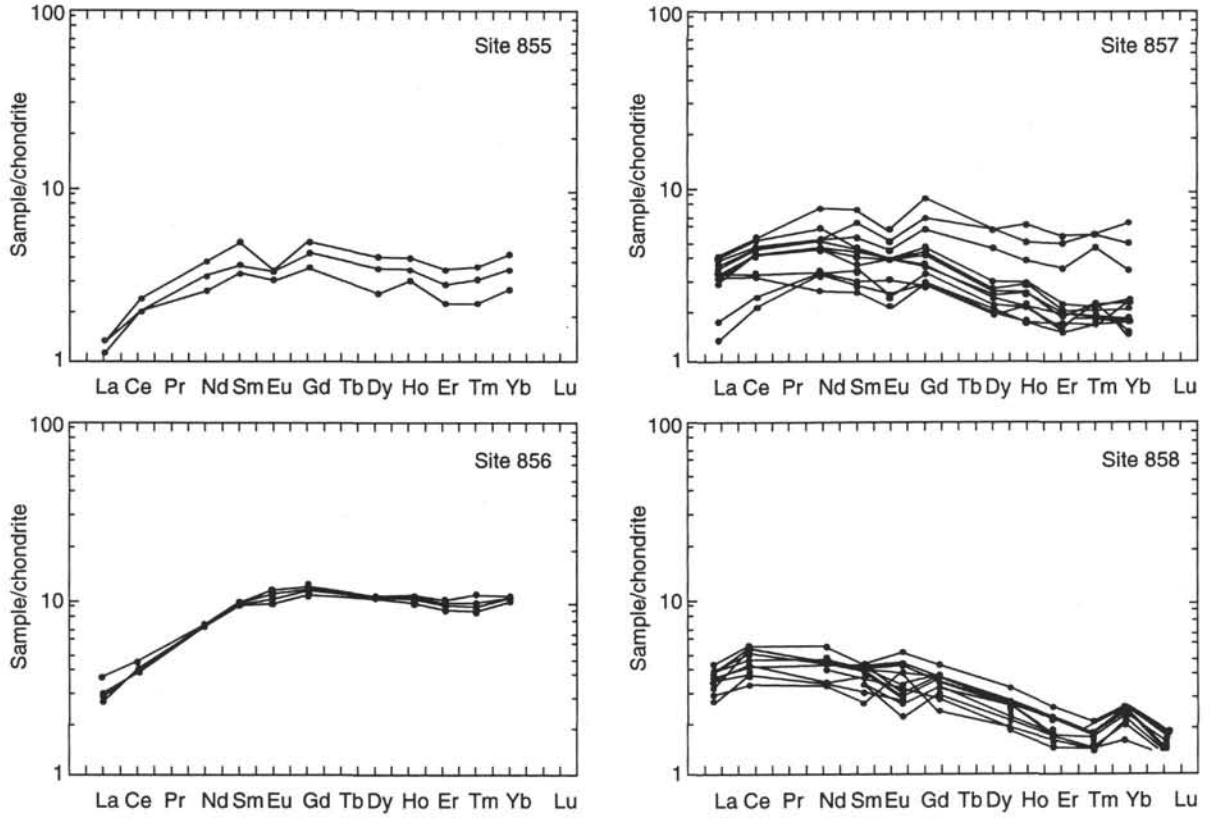

Figure 4. REE compositions for all sites, normalized to chondritic values.

grained diabase is cut by a wairakite-quartz-sphalerite vein that is 1–2 cm thick. Fine-grained basalt is found as a few centimeter-sized fragments in gravel in the upper 5 cm of Section 857C-65R-1 (Unit 9), in contact with a sedimentary horizon. A baked sediment contact above a highly altered basaltic horizon was found at 24 cm depth in Section 857C-66R-1. This basaltic horizon (Unit 10) is unique in that it is a vertical contact between a basaltic intrusion and sediment, either a late crosscutting dike or the toe of a sill. This pale green altered basalt contains chlorite pseudomorphs after olivine or clinopyroxene (probably the latter, given the moderate plagioclase composition) and plagioclase phenocrysts (An60–69). A similar altered basalt fragment is present at the top of Core 857C-67R above a sedimentary horizon. Eighteen centimeters of fine- to medium-grained plagioclase-phyric diabase forms the bottom of Core 857C-67R below the sedimentary horizon (Unit 11). Core 857C-68R (Unit 12) is composed of coarse-grained poikilitic diabase unbroken by any chilled contacts.

Hole 857D

In Hole 857D, mafic sills and interlayered sediment were cored between 581.1 and 936.2 mbsf. Very coarse-grained horizons are fewer in number than recovered in Hole 857C, and several units are composed of only a few pieces of rubble within a mostly sedimentary interval.

The top 110 cm of Core 139-857D-1R-1 (Unit 13) is a fine-grained diabase that terminates with a chilled contact against sediment. Unit 14 is a fine-grained, plagioclase-phyric (An_{69-76}) diabase with a distinct upper contact with sediment at Section 139-857D-1R-2, 65 cm. This unit coarsens slightly in grain-size within Section 857D-2R-1. A few pieces of sedimentary rubble and a chilled contact at Core 857D-2R-1, 47 cm, separate subunits 14A and 14B, which are lithologically identical. This fine- to medium-grained plagioclase-phyric diabase extends to the bottom of Core 857D-3R. Unit 15, in Core 857D-4R, is a heavily veined, coarse-grained diabase that is bounded by sedimentary horizons, although no chilled contacts were recovered. The large grain size suggests that this interval is from the center of a large sill.

The lithology of the igneous intervals in Cores 857D-7R to 857D-9R is a fine- to medium-grain sparsely phyric diabase. This interval comprises subunits 16A–C, which are separated by a chilled margin (Core 857D-8R-1, 0 cm) and a small piece of sediment rubble (Core 857D-8R-1, 66–71 cm), respectively. A partially lithified sedimentary clast is included in the diabase at 857D-8R-1, 34 cm. Subunit 17A has a distinctive chilled and massively altered margin at Section 857D-12R-1, 21 cm, which continuously grades into plagioclase-phyric fine-to medium-grain diabase. In this rock, plagioclase megacrysts (An_{83-94}) are associated with magnesiochromite. This same rock type is found in Subunit 17B, which is composed of a single piece of rubble within sedimentary horizons. Short intervals of fine-grained metadiabase and metabasalt within Sections 857D-15R-1 and 857D-16R-2 constitute subunits 18A and 18B, respectively.

The top of Unit 19 (Section 857D-17R-3) is distinctive in the abundance of large sulfide-filled vesicles or vugs within a leucocratic, fine-grained diabase. Plagioclase displays oscillatory zonation (An_{55-63}) with similar zoning in Mg, Fe, and Ti in the clinopyroxene. This is the thickest unit in this hole, extending through Core 857D-20R, which contains melanocratic ophite with clinopyroxene poikilitically enclosing plagioclase (An_{45-70}) and equant grains of ilmenite. Igneous rock recovered from Sections 857D-21R-1 to 857D-24R-1 (Subunits 20A–D) is leucocratic fine- to medium-grained diabase with local concentrations of plagioclase phenocrysts or embayed megacrysts (An_{77-82}). Short sedimentary intervals separate the subunits; otherwise, they appear to be lithologically identical.

Unit 21 extends from the bottom of Core 857D-24R to the bottom of Core 857D-26R. Except for a fine-grained contact, this unit is a medium-grained diabase with plagioclase glomerocrysts with thin sodic rims. An extensively metamorphosed fine-grained contact zone for Unit 22 is contained within Section 857D-27R-1. This unit is composed of veined and mineralized basaltic rubble and exhibits extensive

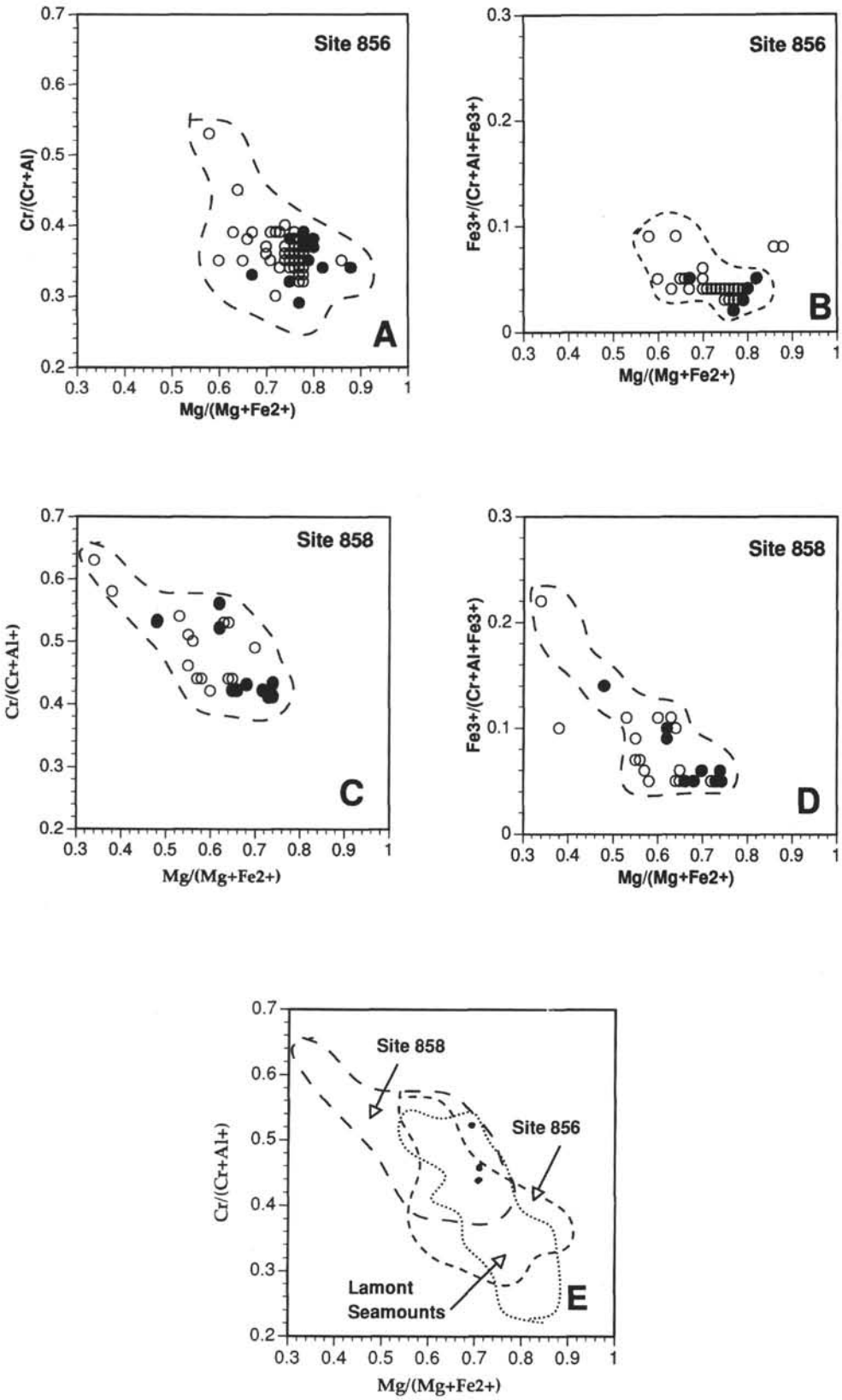

Figure 5. Spinel compositions for Leg 139 basalts. **A.** Cr# vs. Mg# for Site 856. Filled circles are core compositions. **B.** Fe# vs. Mg# for Site 856. Filled circles are core compositions. **C.** Cr# vs. Mg# for Site 858. **D.** Fe# vs. Mg# for Site 858. **E.** Comparison of different sites with Lamont Seamounts. Filled circles are Site 857.

Table 6. Microprobe analyses of chromian spinel compositions, Leg 139, Sites 856–858.

	1[a]	2[b]	3[c]	4[d]	5[e]	6[f]	7[g]	8[h]	9[i]	10[j]	11[k]	12[l]	13[m]	14[n]	15[o]	16[p]	17[q]	18[r]	19[s]	20[t]	21[u]	22[v]	23[w]	24[x]
SiO_2	0.03	0.06	0.05	0.03	0.20	0.73	0.09	0.04	0.22	0.07	0.08	0.14	0.04	0.03	0.03	0.03	0.11	0.14	0.22	0.02	0.03	0.05	0.06	0.15
TiO_2	0.25	0.28	0.27	0.31	0.36	0.89	0.34	0.28	0.26	0.29	0.28	0.32	0.17	0.16	0.15	0.58	1.22	1.25	1.02	0.70	0.74	0.66	0.54	3.33
Al_2O_3	38.01	37.96	37.16	33.55	35.42	22.22	36.47	39.19	37.49	39.16	38.04	37.92	26.30	29.66	31.21	23.20	21.17	20.22	26.15	30.70	29.56	27.97	29.06	13.39
Cr_2O_3	28.80	29.02	29.87	33.26	27.96	38.05	29.86	27.64	29.88	27.97	28.90	29.86	42.13	38.00	35.43	37.75	38.93	38.26	30.63	34.38	34.63	35.13	34.19	34.35
Fe_2O_3	3.98	3.57	3.55	3.51	4.92	7.79	3.77	3.53	3.62	3.52	3.13	4.03	3.12	3.20	3.94	7.30	8.55	8.71	8.56	4.90	4.76	5.97	5.61	16.47
MgO	18.13	18.00	17.68	16.98	13.62	12.17	16.55	17.89	18.34	18.53	17.56	19.03	15.61	15.93	15.83	13.13	13.37	13.13	11.52	15.32	12.91	12.05	12.61	6.49
MnO	0.19	0.22	0.11	0.17	0.24	0.31	0.24	0.14	0.15	0.10	0.10	0.11	0.14	0.18	0.19	0.19	0.25	0.28	0.27	0.16	0.21	0.22	0.21	0.56
FeO	9.81	9.94	10.43	10.68	16.17	15.99	11.98	10.39	9.59	9.45	10.65	9.23	12.00	11.81	12.18	14.16	14.54	15.01	15.89	12.94	16.48	17.62	16.81	22.53
Total	99.20	99.05	99.12	98.49	98.89	98.16	99.30	99.12	99.55	99.09	98.74	100.64	99.51	98.96	98.96	96.31	98.14	97.00	94.26	99.12	99.32	99.66	99.10	97.26
Si	0.007	0.013	0.011	0.008	0.047	0.183	0.022	0.009	0.049	0.017	0.018	0.032	0.01	0.006	0.006	0.007	0.024	0.032	0.056	0.004	0.007	0.012	0.013	0.040
Ti	0.043	0.048	0.046	0.055	0.064	0.168	0.058	0.048	0.044	0.048	0.048	0.056	0.03	0.028	0.027	0.110	0.224	0.240	0.192	0.125	0.134	0.121	0.099	0.683
Al	10.118	10.123	9.954	9.194	9.801	6.558	9.843	10.406	9.950	10.361	10.189	9.904	7.42	8.275	8.663	6.916	6.192	6.056	7.752	8.547	8.378	8.002	8.293	4.305
Cr	5.143	5.193	5.368	6.115	5.190	7.534	5.407	4.924	5.320	4.964	5.193	5.232	7.97	7.112	6.598	7.549	7.960	7.680	6.088	6.421	6.584	6.742	6.544	7.410
Fe	0.677	0.608	0.607	0.613	0.869	1.469	0.650	0.598	0.614	0.594	0.536	0.672	0.56	0.570	0.698	1.389	1.600	1.664	1.616	0.871	0.862	1.090	1.023	3.381
Mg	6.109	6.070	5.990	5.883	4.765	4.543	5.650	6.009	6.154	6.199	5.948	6.288	5.57	5.621	5.559	4.951	4.944	4.968	4.320	5.396	4.626	4.361	4.540	2.641
Mn	0.037	0.042	0.021	0.034	0.047	0.065	0.046	0.026	0.029	0.019	0.019	0.024	0.03	0.036	0.038	0.040	0.056	0.064	0.056	0.031	0.042	0.044	0.043	0.129
Fe	1.854	1.881	1.982	2.076	3.174	3.348	2.294	1.958	1.806	1.773	2.024	1.712	2.40	2.338	2.400	2.995	3.016	3.184	3.824	2.557	3.314	3.578	3.403	5.140
Catsum	23.987	23.977	23.979	23.977	23.958	23.868	23.970	23.978	23.965	23.976	23.975	23.920	23.985	23.987	23.988	23.956	24.016	23.888	23.904	23.952	23.947	23.950	23.958	23.729
Cr/(Cr + Al)	0.337	0.339	0.350	0.399	0.346	0.535	0.355	0.321	0.348	0.324	0.338	0.346	0.518	0.462	0.432	0.522	0.562	0.559	0.440	0.429	0.440	0.457	0.441	0.633
Mg/(Mg + Fe)	0.767	0.763	0.751	0.739	0.600	0.576	0.711	0.754	0.773	0.778	0.746	0.786	0.699	0.706	0.698	0.623	0.621	0.609	0.530	0.678	0.583	0.549	0.572	0.339
$Fe_3/(Cr + Al + Fe_3)$	0.042	0.038	0.038	0.039	0.055	0.094	0.041	0.038	0.039	0.037	0.034	0.043	0.035	0.036	0.044	0.088	0.102	0.108	0.105	0.055	0.054	0.069	0.064	0.224
LIQ Mg/Fe	2.11	2.06	1.97	2.00	1.00	1.28	1.62	1.91	2.21	2.18	1.86	2.38	1.95	1.85	1.72	1.52	1.67	1.56	0.94	1.62	1.09	0.99	1.05	0.71
Liquid Mg#	0.68	0.67	0.66	0.67	0.50	0.56	0.62	0.66	0.69	0.69	0.65	0.70	0.66	0.65	0.63	0.60	0.63	0.61	0.49	0.62	0.52	0.50	0.51	0.41

[a] 139-856A-14X-1, 68–70 cm, core, large euhedral grain.
[b] 139-856A-14X-1, 68–70 cm, rim, large euhedral grain.
[c] 139-856A-14X-1, 68–70 cm, large euhedral megacryst.
[d] 139-856A-14X-1, 68–70 cm, small groundmass grain.
[e] 139-856A-14X-1, 68–70 cm, rim, large grain.
[f] 139-856A-14X-1, 68–70 cm, rim, small groundmass grain.
[g] 139-856A-14X-1, 116–118, rim.
[h] 139-856A-14X-1, 116–118, core, previous grain.
[i] 139-856B-8H-CC, 1–3 cm, core, large grain.
[j] 139-856B-8H-CC, 1–3 cm, rim, large grain.
[k] 139-856B-9H-1, 4–8 cm, rim, medium grain.
[l] 139-856B-10H-1, 64–67 cm, outer zone.
[m] 139-857D-12R-1, 51–53 cm, core, euhedral grain.
[n] 139-857D-12R-1, 51–53 cm, rim, euhedral grain.
[o] 139-857D-12R-1, 51–53 cm, small euhedral grain.
[p] 139-858F-29R-1, 27–39 cm, small grain in chlorite pseudomorph.
[q] 139-858G-3R-1, 24–25 cm.
[r] 139-858G-3R-1, 24–25 cm, may be altered.
[s] 139-858G-3R-1, 24–25 cm, may be altered.
[t] 139-858G-16R-1, 81–83 cm, core, large euhedral grain.
[u] 139-858G-16R-1, 81–83 cm, middle, large euhedral grain.
[v] 139-858G-16R-1, 81–83 cm, rim, large euhedral grain.
[w] 139-858G-16R-1, 81–83 cm, core, large grain.
[x] 139-858G-16R-1, 81–83 cm, rim, strongly zoned grain.

Table 7. Microprobe analyses of oxide minerals, Leg 139.

A. Composition of titanomagnetite Site 856.

Core section interval (cm)	TiO_2	Al_2O_3	Cr_2O_3	V_2O_3	Fe_2O_3	FeO	FeO[t]	MnO	NiO	ZnO	Total	Si	Ti	Al	Cr	V	Fe^{3+}	Fe^{2+}	Mn	Mg	Ca	Ni	Zn	Total
139-856A-																								
14X, 90–92	20.22	1.41	0.04	0.46	25.69	47.53	70.65	1.41	0.05	0.17	96.63	0.000	0.587	0.064	0.001	0.021	0.746	1.535	0.046	0.000	0.000	0.002	0.005	3.007
14X, 90–92	18.05	1.65	0.01	0.93	30.41	46.92	74.28	0.58	0.23	0.05	98.90	0.000	0.515	0.074	0.000	0.042	0.868	1.488	0.019	0.000	0.000	0.007	0.001	3.014
14X, 7–9	20.65	1.82	0.54	0.57	24.57	48.36	70.47	1.44	0.02	0.19	98.00	0.000	0.591	0.082	0.016	0.026	0.703	1.538	0.046	0.000	0.000	0.001	0.005	3.009
14X, 7–9	20.08	1.85	0.28	0.43	25.82	47.85	71.08	1.33	0.02	0.18	97.69	0.000	0.577	0.083	0.008	0.020	0.742	1.528	0.043	0.000	0.000	0.001	0.005	3.007
14X, 7–9	19.15	1.85	0.00	0.49	27.30	46.76	71.23	1.43	0.03	0.15	96.55	0.000	0.555	0.084	0.000	0.023	0.791	1.503	0.047	0.000	0.000	0.001	0.004	3.008

B. Composition of ilmenite Site 857.

Core section interval (cm)	SiO_2	TiO_2	Al_2O_3	Cr_2O_3	V_2O_3	Fe_2O_3	FeO	FeO[t]	MnO	MgO	CaO	Total	Si	Ti	Al	Cr	V	Fe^{3+}	Fe^{2+}	Mn	Mg	Ca	Total	X'ilm
139-857C-																								
59R-2, 62–64	0.04	47.36	0.16	0.01	0.68	8.51	38.90	46.56	3.32		0.29	99.32	0.001	0.908	0.005	0.000	0.014	0.163	0.829	0.072	0.000	0.008	2.000	0.828
59R-2, 62–64	0.08	48.08	0.09	0.00	0.41	7.03	39.46	45.78	3.46		0.29	98.96	0.002	0.925	0.003	0.000	0.008	0.135	0.844	0.075	0.000	0.008	2.000	0.842
59R-2, 94–96	0.06	47.68	0.19	0.06	0.49	7.64	39.41	46.28	3.11		0.30	98.97	0.002	0.916	0.006	0.001	0.010	0.147	0.842	0.067	0.000	0.008	2.000	0.841
59R-4, 35–37	0.08	47.21	0.10	0.02	0.49	8.16	37.96	45.31	4.20		0.26	98.60	0.002	0.912	0.003	0.000	0.010	0.158	0.816	0.091	0.000	0.007	2.000	0.814
59R-4, 35–37	0.05	47.37	0.14	0.00	0.61	8.71	37.87	45.70	4.42		0.24	99.49	0.001	0.907	0.004	0.000	0.012	0.167	0.806	0.095	0.000	0.007	2.000	0.805
60R-1, 173–175	0.13	46.87	0.11	0.01	0.51	9.85	35.48	44.35	5.89		0.67	99.54	0.03	0.896	0.003	0.000	0.010	0.188	0.754	0.127	0.000	0.018	2.000	0.751
60R-1, 173–175	0.10	44.84	0.20	0.02	0.62	12.89	33.87	45.47	5.53		0.76	98.97	0.003	0.864	0.006	0.000	0.013	0.248	0.725	0.120	0.000	0.021	2.000	0.723
62R-1, 20–22	0.01	50.97	0.10	0.03		4.00	35.53	39.14	9.72	0.17	0.13	100.59	0.000	0.960	0.003	0.001	0.000	0.075	0.744	0.206	0.003	2.000	0.744	
62R-2, 7–9	0.02	47.63	0.08	0.00	0.19	7.95	34.91	42.06	7.55		0.23	98.71	0.001	0.920	0.002	0.000	0.004	0.154	0.749	0.164	0.000	0.006	2.000	0.749
62R-2, 7–9	0.06	47.65	0.09	0.03	0.15	7.62	34.55	41.41	7.90		0.29	98.44	0.002	0.922	0.003	0.001	0.003	0.147	0.743	0.172	0.000	0.008	2.000	0.741
62R-2, 7–9	0.00	47.86	0.09	0.02	0.06	7.57	34.39	41.20	8.19		0.28	98.59	0.000	0.925	0.003	0.000	0.001	0.146	0.739	0.178	0.000	0.008	2.000	0.739
63R-1, 69–71	0.10	47.87	0.08	0.00	0.11	7.05	33.90	40.25	8.58		0.45	98.23	0.003	0.927	0.002	0.000	0.002	0.137	0.730	0.187	0.000	0.012	2.000	0.727
68R-1, 12–14	0.01	48.81	0.11	0.03	0.40	5.99	34.15	39.54	9.17		0.37	99.07	0.000	0.936	0.003	0.001	0.008	0.115	0.728	0.198	0.000	0.010	2.000	0.728
68R-1, 12–14	0.04	48.38	0.23	0.00	0.34	6.65	33.73	39.71	9.48		0.17	99.06	0.001	0.928	0.007	0.000	0.128	0.720	0.205	0.000	0.005	2.000	0.719	
68R-1, 90–92	0.08	47.39	0.26	0.03	0.56	8.82	32.75	40.69	9.57		0.21	99.77	0.002	0.904	0.008	0.001	0.011	0.168	0.695	0.206	0.000	0.006	2.000	0.693
139-																								
6R-1, 71–76	0.03	50.50	0.08	0.01		4.92	42.42	46.84	2.78	0.07	0.07	100.76	0.001	0.952	0.002	0.000	0.000	0.093	0.889	0.059	0.003	0.002	2.000	0.888
6R-1, 71–76	0.06	50.82	0.07	0.03		4.61	42.64	46.79	2.80	0.10	0.09	101.04	0.001	0.954	0.002	0.001	0.000	0.087	0.890	0.059	0.004	0.002	2.000	0.889
8R-1, 96–98	0.10	49.79	0.09	0.00		6.09	38.55	44.03	5.62	0.10	0.37	100.61	0.003	0.939	0.003	0.000	0.115	0.808	0.119	0.004	0.004	0.010	2.000	0.806
24R-1, 115–117	0.19	49.19	0.04	0.00		5.19	38.70	43.38	5.22	0.17	0.13	98.69	0.005	0.945	0.001	0.000	0.000	0.100	0.827	0.113	0.006	0.004	2.000	0.822
24R-1, 115–117	0.08	50.41	0.04	0.01		4.62	38.42	42.58	5.97	0.16	0.53	100.13	0.00	0.954	0.001	0.000	0.000	0.088	0.808	0.127	0.006	0.014	2.000	0.806
25R-1, 64–66	0.06	50.70	0.03	0.00		4.65	41.86	46.05	3.38	0.12	0.13	100.79	0.002	0.954	0.001	0.000	0.000	0.088	0.876	0.072	0.004	0.003	2.000	0.875
25R-1, 64–66	0.05	50.76	0.07	0.02		4.25	41.73	3.49	0.13	0.16	100.56	0.001	0.957	0.002	0.002	0.000	0.000	0.080	0.875	0.074	0.005	0.004	2.000	0.874
26R-1, 76–78	0.07	50.89	0.07	0.00		4.18	38.21	41.97	6.82	0.13	0.39	100.62	0.002	0.958	0.002	0.000	0.000	0.079	0.800	0.145	0.005	0.010	2.000	0.798

C. Composition of magnetite Site 858.

Core section interval (cm)	TiO_2	Al_2O_3	Cr_2O_3	Fe_2O_3	FeO	FeO[t]	MnO	MgO	Total	Ti	Al	Cr	Fe^{3+}	Fe^{2+}	Mn	Mg	Total
139-857F-																	
27R-1, 42–43	0.320	0.250	0.000	65.427	30.016	88.890	0.030	0.080	95.520	0.010	0.012	0.000	1.969	1.004	0.001	0.005	3.000
27R-1, 42–43	0.780	0.190	0.060	64.839	30.562	88.907	0.050	0.070	95.990	0.023	0.009	0.002	1.9423	1.018	0.002	0.004	3.000
27R-1, 42–43	0.990	0.330	0.060	63.166	29.937	86.777	0.060	0.260	94.040	0.030	0.016	0.002	1.922	1.012	0.002	0.016	3.000

Notes: Structural formula calculated on the basis of four oxygens with calculated values of Fe^{3+} and Fe^{2+}. FeO is total iron calculated as FeO. Fe_2O_3, FeO, Fe^{3+}, and Fe^{2+} are calculated by stoichiometry. X'ilm is mole fraction ilmenite in mineral.

Table 8. Microprobe analyses of sulfide minerals, Leg 139, Site 856.

A. Pyrrhotite and pentlandite compositions.

Core, section, interval (cm)	Cu	Fe	Ni	S	Total	Fe mole	Ni mole	S mole	Cu mole	Fe mole %	Ni mole %	S mole %	Total
139-856A-													
14X-1, 7–9	0.01	31.31	36.17	32.75	100.26	0.561	0.616	1.020	0.000	0.255	0.280	0.464	1.000
14X-1, 7–9	0.00	60.16	0.83	39.75	100.76	1.078	0.014	1.238	0.000	0.463	0.006	0.531	1.000
14X-1, 90–92	0.06	33.44	33.11	33.16	99.77	0.599	0.564	1.033	0.001	0.273	0.257	0.470	1.000
14X-1, 90–92	3.64	54.10	4.84	36.86	99.46	0.970	0.082	1.148	0.057	0.429	0.037	0.509	0.975
14X-1, 90–92	0.00	57.49	3.07	38.53	99.10	1.030	0.052	1.200	0.000	0.451	0.023	0.526	1.000
14X-1, 90–92	0.10	60.15	1.12	39.05	100.44	1.078	0.019	1.217	0.002	0.466	0.008	0.525	0.999
14X-1, 90–92	0.08	59.99	1.08	38.65	99.83	1.075	0.018	1.204	0.001	0.468	0.008	0.524	0.999
14X-1, 90–92	0.00	60.85	0.51	37.64	99.01	1.091	0.009	1.173	0.000	0.480	0.004	0.516	1.000
139-856B-													
1H-1, 48–50	0.97	60.13	0.00	38.75	100.55	1.078	0.000	1.207	0.015	0.467	0.000	0.523	0.990
1H-1, 48–50	0.37	60.48	0.02	38.77	100.58	1.084	0.000	1.208	0.006	0.470	0.000	0.523	0.993

B. Copper minerals.

Core, section, interval (cm)	Cu	Fe	Mn	Zn	Cd	S	Total	Cu mole	Fe mole	S mole	Fe mole %	S mole %
139-856A-												
14X-1, 90–92	33.79	31.00	0.00	0.17	0.00	34.62	99.58	0.532	0.556	1.079	0.256	0.497
14X-1, 90–92	33.96	31.00	0.03	0.14	0.01	34.45	99.59	0.535	0.556	1.073	0.257	0.496
14X-1, 90–92	33.76	30.46	0.02	0.20	0.00	34.35	98.79	0.532	0.546	1.070	0.254	0.498

replacement of plagioclase (An_{53-69}) by chlorite. Some pieces are very coarse-grained and presumably come from highly altered centers of large (fractured?) sills. Section 857D-29R-1 (Subunit 23A) is a highly epidotized diabase that systematically increases in grain size from top to bottom. Strongly zoned plagioclase (An_{66-49}) is partially replaced by quartz and epidote. This unit is adjacent to intervals of epidote-rich sandstone. Cores 857D-30R to 857R-32R (Subunits 23B–G) are similar epidotized and chloritized fine-grained diabase, with intervening sediment and bleached metabasalt contact zones separating subunits. The pieces are small and discontinuous and may be a series of thin, highly fractured sills.

A conspicuous quenched margin for Unit 24 was observed in Core 857D-33R-1, with a bleached contact zone and inner vesicle-rich zone that grades rapidly into a medium-grained diabase. Subunit 25A is a single piece of variolitic basalt in Core 139-34R-1. Subunits 25B (Core 139-35-1, 0 cm to 139-36-1, 22 cm) and 25C (Core 139-36R-1, 32 cm to 139-36-1, 143 cm) are similarly fine-grained diabase; they increase in grain size and become more mafic toward their bases to ophitic textures with some poikilitic clinopyroxenes. In subunit 25B, plagioclase (An_{34-72}) is altered to quartz and albite. In subunit 25C, plagioclase (An_{45-68}) shows normal, reversed and oscillatory zonation and replacement by epidote. Unit 26 (139-37R-1, 17–20 cm) is a small single piece of epidotized diabase within a sedimentary interval.

Petrography and Mineral Chemistry

No fresh olivine was observed in any of the sills, although small euhedral pseudomorphs are interpreted to be replacements of either olivine or clinopyroxene. The mafic pseudomorphs are composed of smectite/chlorite or chlorite. In one unit they are associated with spinel, in which they likely are replacements of olivine.

Spinel was observed in only one thin section from Unit 17A. It has a Cr# (=Cr/Cr+Al) = 0.52–0.43 and a Mg# (=Mg/Mg+Fe) = 0.70–0.71 (Table 6). This spinel occurs as strongly zoned euhedral crystals in a sill containing unusually calcic plagioclase. The sill occurs at the stratigraphic horizon of the most intense alteration that may be associated with a fault.

The Fe-oxide phase in the Site 857 sills is dominated by ilmenite (Table 7) with sparse magnetite and no titanomagnetite, in contrast to the samples from Site 856. The ilmenite is observed as interstitial anhedral grains in the finer-grained portions of the sills and as spectacular euhedral or skeletal tabular plates in the coarser-grained portions of the sills. Ilmenite together with its alteration products, makes up

Table 9. Unit designations for igneous rocks from Site 857.

Unit	Top	Bottom
139-857C-		
1	59R-1, 0 cm	59R-4, 139 cm
2	60R-1, 0 cm	60R-2, 31cm
3	60R-2, 49 cm	60R-2, 142 cm
4	61R-1, 0 cm	61R-1, 100 cm
5	61R-2, 0 cm	61-2, 82 cm
6	62R-1, 0 cm	62R-2, 79 cm
7	63R-1, 34 cm	63R-1, 73 cm
8	64R-1, 0 cm	64R-2, 133 cm
9	65R-1, 0 cm	65-1, 5 cm
10	66R-1, 24 cm	67-1, 5 cm
11	67R-1, 58 cm	67R-1, 76 cm
12	68R-1, 0 cm	68R-3, 36 cm
139-857D-		
13	1R-1, 0 cm	1R-1, 110 cm
14A	1R-2, 65 cm	2R-1, 38 cm
14B	2R-1, 47 cm	3R-2, 123 cm
15	4R-1, 7 cm	4R-2, 89 cm
16A	7R-1, 0 cm	7R-1, 52 cm
16B	8R-1, 0 cm	8R-1, 66 cm
16C	8R-1, 71 cm	9R-1, 122 cm
17A	12R-1, 21 cm	12R-2, 133 cm
17B	13R-1, 7 cm	13R-1, 12 cm
139-857D-		
18A	15R-1, 35 cm	15R-1, 63 cm
18B	16R-2, 55 cm	16R-2, 65 cm
19	17R-3, 48 cm	20R-1, 119 cm
20A	21R-1, 18 cm	21R-1, 115 cm
20B	21R-1, 135 cm	21R-1, 140 cm
20C	22R-1, 0 cm	22R-1, 14 cm
20D	22R-1, 31 cm	24R-1, 12 cm
21	24R-1, 104 cm	26R-1, 96 cm
22	27R-1, 17 cm	28R-1, 7 cm
23A	29R-1, 32 cm	29R-2, 44 cm
23B	30R-1, 16 cm	30R-1, 19 cm
23C	30R-1, 25 cm	30R-1, 36 cm
23D	30R-1, 39cm	31R-1, 4 cm
23E	31R-1, 53 cm	31R-1, 91 cm
23F	31R-1, 91 cm	31R-1, 108 cm
23G	32R-1, 0 cm	32R-1, 65 cm
24	33R-1, 18 cm	33R-1, 98 cm
25A	34R-1, 88 cm	34R-1, 95 cm
25B	35R-1, 0 cm	36R-1, 22 cm
25C	36R-1, 32 cm	36R-1, 143 cm
26	37R-1, 17 cm	37R-1, 20 cm

about 3% of the rock. The average ilmenite composition is $Fe_{0.90}Ti_{0.93}Mn_{0.12}O_3$. The manganese contents of these ilmenite grains is unusually high (average 6.1 wt%) if compared with typical ilmenite compositions (Haggerty, 1976). The ilmenite in sills from 470 to 510 mbsf have progressively increasing Mn contents. Magnetite was observed as anhedral grains that were frequently altered or completely replaced, presumably by sulfide. No microprobe analyses were obtained.

Plagioclase is present as zoned phenocrysts or microphenocrysts intergrown with clinopyroxene (Table 4). In Hole 857D, large plagioclase megacrysts are also present with compositions varying from An_{80-89} (Table 4). Zoned phenocrysts have core compositions varying from An_{60-73}. Plagioclase contained in poikilitic intergrowths with pyroxene tend to show less chemical zonation and presumably preserve primary compositions. The rims of the phenocrysts and the compositions of the microphenocrysts are more sodic, averaging An_{50-60}. Sodic compositions observed as rims on phenocrysts or patches in altered microphenocrysts may not be primary, but are typically An_{40-50}. Although many of the plagioclase crystals show conspicuous optical zonation and replacement by secondary minerals, including chlorite and epidote, albitic rims on plagioclase (An <20) are relatively rare. Albitic compositions were only analyzed in two samples from the bottom of Hole 857D from Units 25B and 25C. Small patches of albitic plagioclase were rarely observed as anhedral relicts within masses of chloritic replacements (?) 140–142 cm, (pc. 6) with An_{12-15}). Extreme plagioclase values (An_{95-83}) have also been observed for megacrysts in Unit 17A. It is notable that these are associated with magnesiochromite, suggesting an unusually primitive magmatic composition for this unit or that the megacrysts are not related to the host magma.

Clinopyroxene is present as large phenocrysts intergrown with included plagioclase in an ophitic texture, as small barrel-shaped microphenocrysts, and as granular to spherulitic groundmass phases (Table 5). The clinopyroxene is highly variable in composition with both normal and reversed zonation in Al, Cr, and Ti contents common (Table 5). Cores of poikilitic clinopyroxenes are typically aluminous with Al_2O_3 >4%. Many of these also have high Cr contents with Cr_2O_3 >1%. Rims of zoned pyroxene crystals are normal augite with Al_2O_3 of 2%–3% and Cr <0.8%. Brownish rims of pyroxene also contain high Ti (>1%). These rims are frequently observed on pyroxenes intergrown with plagioclase either poikilitically enclosing plagioclase or as symplectites. Less commonly, rims on pyroxenes are subcalcic augites with Al_2O_3 <2% and CaO <19% (e.g., Sample 139-857C-60R-2, 17–19 cm, [piece 1]). These subcalcic augites are high in FeO and low in Cr_2O_3 and TiO_2, suggesting a highly evolved magmatic composition with ilmenite on the liquidus. In contrast, groundmass clinopyroxene commonly contains high Al_2O_3 (up to 6%) and TiO_2 (over 3%) (e.g., Sample 139-857C-66R-1, 108–110 cm [piece 16]). This latter sample is from a highly altered crosscutting dike that forms Unit 10. These variations in clinopyroxene chemistry are interpreted to represent both variable primary magma composition and the effect of extremely variable cooling rates for the magmas once intruded into the sediment.

The principal sulfide minerals are pyrite, pyrrhotite, chalcopyrite, isocubanite, and sphalerite, all of which are interpreted to be secondary in origin. These occur as aggregates disseminated throughout the bulk of the rock and as vein fillings that precipitated from hydrothermal fluids. Pyrrhotite occurs more predominantly in the lower sills in Site 857. The nickel content of pyrrhotite, although variable, is high, typically ranging from 0.18% to 2.01%. Two analyses from Sample 139-857D-26R-1, 76–78 cm, contain 10.2% and 12.4% Ni, representing exceptional amounts of nickel for pyrrhotite. Nickel is bimodally distributed in pyrrhotite; low molar percent (mol%) Fe pyrrhotite (less than 46 mol% Fe) contains a uniform amount of nickel (1.4 mol%), whereas high Fe-pyrrhotite (>46 mol% Fe) contains only about 0.5 mol% Ni. Although the distribution and textures of the pyrrhotite grains in Site 857 sills generally indicate that they have been deposited after the rock was completely crystallized, their high nickel content may indicate that they have a magmatic parent.

Alteration of the Site 857 Sill Complex

The sills recovered from Site 857 are variably metamorphosed and interlayered with altered or indurated sediment. Fine-grained quenched sill margins exhibit intense hydrothermal recrystallization and are extensively metasomatised. Such margins are bleached to a pale gray and are completely replaced by pale magnesian chlorite (Mg/Fe >2) with quartz and titanite. These are anomalously high in Mg, Al, and Ti compared to less-altered samples. Included microlites and phenocrysts are replaced, predominantly by green chlorite and epidote joined by actinolite in the lower half of Hole 857D. The most abundant and largest vein networks crosscut these highly altered margins and extend into the fresher rock slightly beyond the extent of the chill. Typical vein fillings include green ferroan chlorite/smectite, sulfide minerals, quartz, zeolites (most notably wairakite with Ca/Ca+Na = 95) and epidote (Ps_{8-30}, including thulite with Mn >1%). The chilled margins of the sills and the immediately adjacent interval typically are vesicle-rich. The vesicles are almost all filled, most frequently with green ferroan chlorite, but also with quartz, epidote, prehnite, smectite, or sulfide minerals.

The second most intensely metamorphosed intervals are the coarse-grained sill interiors. The quantity of chloritic replacement of mesostasis and crystals is variable, with some intervals exhibiting over 50% replacement. The igneous plagioclase is strongly zoned and includes replacement by a variety of minerals including sodic plagioclase, epidote, chlorite, and prehnite. White sodic rims and mottled extinction in the plagioclase phenocrysts suggest that these are partially replaced by sodic plagioclase, yet abundant albite was not detected by microprobe. Much of the strong zonation in the plagioclase could in fact be primary. Pervasive alteration is best developed in Hole 857D where chlorite, epidote, and titanite are consistently present in greater abundances than observed in Hole 857C, and are the dominant vein minerals. The least-altered rocks are fine-to-medium grained diabase not associated with chilled margins. The alteration in the freshest intervals is limited to replacement of the sparse amounts of mesostasis.

Prehnite occurs in Unit 14B, both filling veins and replacing plagioclase. A substantial mass flux of Ca is suggested by the abundance of calcic vein minerals. Similarly the mass flux of magnesium is evidenced by the abundance of chlorite and the spuriously high Mg numbers (Table 1; Fig. 2) based on the whole-rock chemistry.

The whole-rock chemistry for all of the sills reflects the impact of this pervasive alteration, with total volatile content (H_2O + S, or LOI) ranging from 1.3 to 8.4 wt%. Oxygen isotopic analyses of whole-rock powders vary from $\delta^{18}O$ = 2.5–4.5‰, suggesting alteration at temperatures above 250°C (Table 2). These extremely depleted values for $\delta^{18}O$ probably reflect the abundance of chlorite and formation of secondary sodic plagioclase (Stakes, unpubl. data). The most highly altered samples are in the uppermost section of sill, between 450 and 650 mbsf. This area is coincident with a high deformation zone (fractures and faulted rocks), and is also distinguished by a much higher content of veins.

Geochemistry

Alteration has undoubtedly modified the MgO and CaO contents and possibly other constituents in many if not all of these samples. MgO content does correlate with H_2O in the overall data set, and correlates poorly with Ni (r = 0.5). These are the expected relationships if Mg was added from seawater during alteration, as no corresponding nickel would be added. In addition, the calculated Mg numbers are extremely high and are inconsistent with the mineralogy as well as the calculated magma Mg# from the spinel in Unit 17. This suggests the addition of seawater MgO. In an attempt to determine some aspects of the primary igneous nature of these rocks, a subset of "least altered samples" was established. These 21 samples have less than 3.0% total volatile content; included in these are samples with

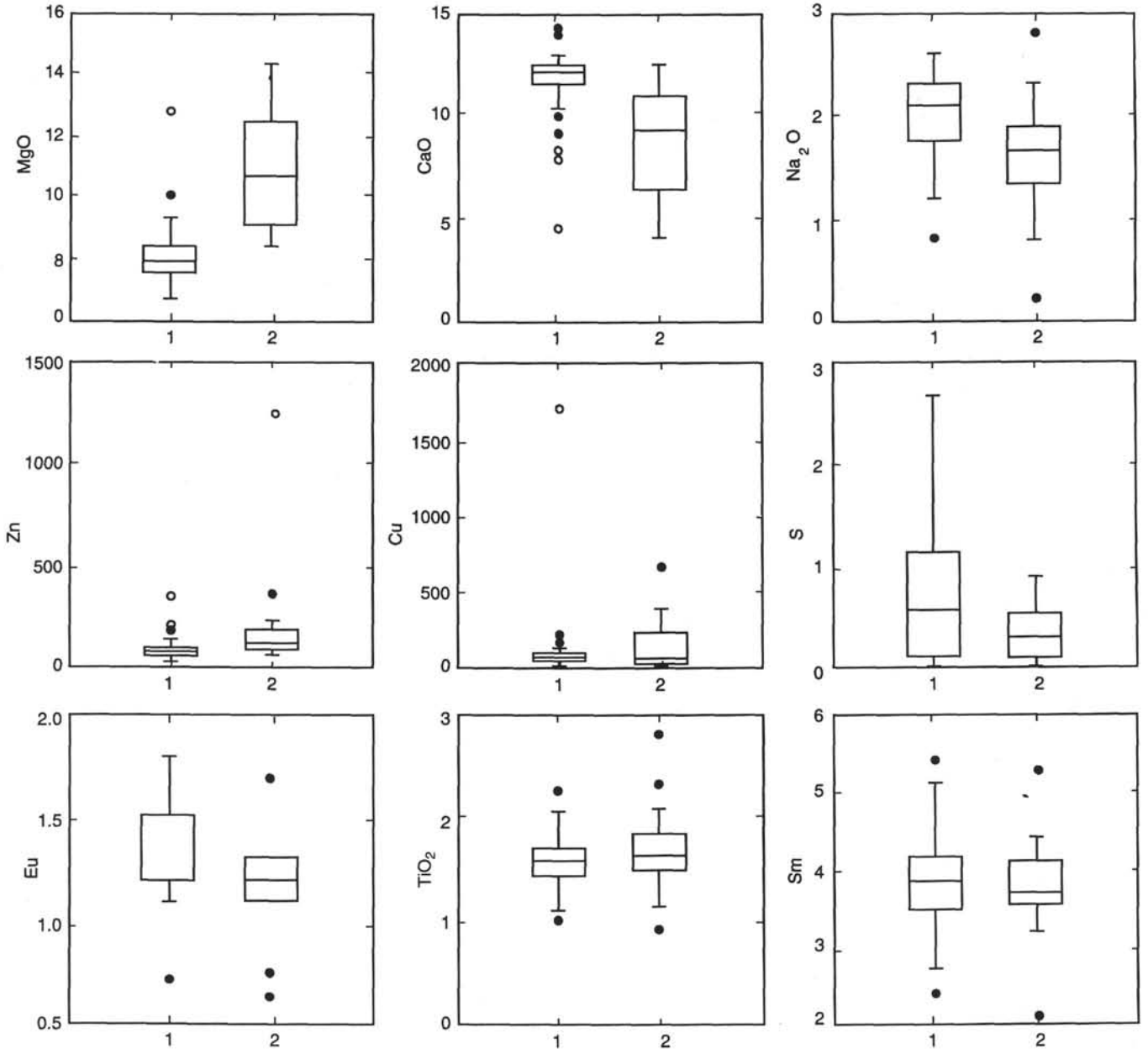

Figure 6. Box plots comparing selected major and trace elements compositions of "unaltered" (Group 1) and "altered" (Group 2) samples, chosen as described in text.

less than 0.9% total sulfur. A comparison of "unaltered" (Group 1) and "altered" (Group 2) data sets is provided in Figure 6. The unaltered subset is significantly lower in MgO and significantly higher in CaO than the altered samples. In eliminating samples with volatile contents higher than 3%, it is possible that a few samples with higher primary ferromagnesian contents may have been excluded. For example, the spinel-bearing sill was not included in the unaltered subset although it is likely one of the most primitive units sampled at this site. In the filtered data set, Ni correlates moderately well with MgO ($r = 0.8$), an expected primary igneous relationship. Thus the filtered data set is a fair representation of primary igneous compositions, diluted by addition of H_2O, but likely not affected in a major way by Mg addition. This filtering puts an upper limit on total MgO content of about 9.5 wt%. Thus it is likely that any samples containing more than this content of MgO are highly altered and of little use in determining primary igneous petrochemical trends.

Examination of the sulfur distribution in the "unaltered" suite of samples indicates a bimodal sulfur distribution. One population contains samples with a maximum of 1800 ppm sulfur, the other from 1800–9000 ppm. The latter group of samples have had much sulfur added and thus have been somewhat altered. In considering whether to eliminate these high sulfur samples from the "unaltered" population, we examined the compositional changes between a sample suite (nine samples) containing low (<0.13%) S, a larger suite (the "unaltered" suite determined above) containing <3.0% total volatile content (21 samples), and the total suite of samples. The average copper content of the overall sample population is about 45% higher (125 ppm) than the "unaltered" and low-S suite (90 and 85 ppm, respectively), but virtually identical in the latter two suites. Zinc shows a gradual increase, from 74 ppm for the low-S suite, to 91 for the "unaltered" suite, to 102 ppm for the total suite. The "immobile" elements (TiO_2, Cr, Ni, Y, Yb, Zr, and the REEs) do not differ significantly between the total suite of samples and the "unaltered" suite of 21 samples. Thus for petrochemical considerations using these elements, we use the full suite of analyses; when using the major elements, the "unaltered" suite is used.

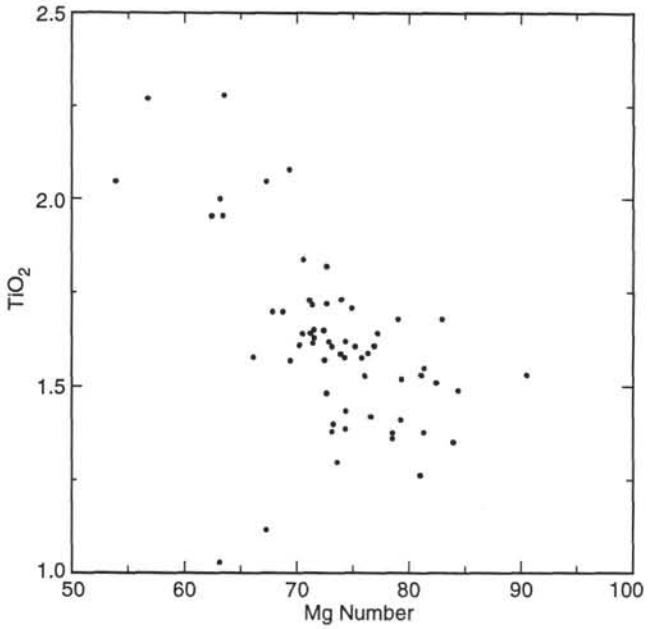

Figure 7. TiO_2 Mg number for samples from Site 857 with total volatiles <3% ("unaltered suite"), including shipboard data. Note variation in TiO_2 at single value of Mg number.

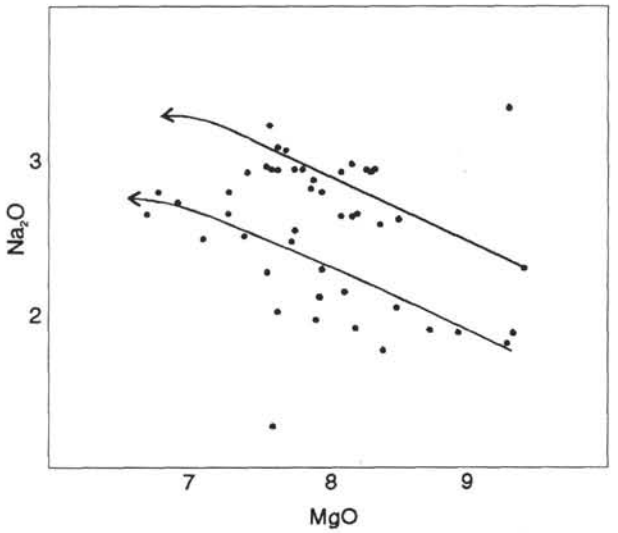

Figure 8. MgO vs. Na_2O for "unaltered" suite of samples from Site 857 sills. Two fractionation trends are defined, suggesting two parent magmas for these sills.

Major Element Data

For the complete set of data (Fig. 2), the range of Na_2O values is less than that of Site 858 and Site 855, suggesting little uptake of Na_2O due to alteration. Relative to average MORB, the rocks are substantially depleted in K due to alteration. In the sediments, K, Rb, and Ba are completely removed by hydrothermal alteration (see Goodfellow and Peter, this volume).

The plot of TiO_2 vs. Mg number, using both shipboard and new data filtered to remove the most-altered samples (Fig. 7) illustrates that these samples form a grossly linear trend due to crystal fractionation. However, samples show considerable variation in TiO_2 at the same Mg#, suggesting separate magma fractionation series from different parental magmas. This suggests that the sill complex may be composed of magmas resulting from variable degrees of partial melting and may not be contemporaneous. Similarly, on a plot of Na_2O vs. MgO (Fig. 8), the filtered data form two subparallel trends similar to the liquid lines of descent calculated by Klein and Langmuir (1987). Both lines indicate low-pressure fractionation, possibly from two parent magmas. A high-and-low Fe trend is similarly seen in Fe_2O_3 vs. Mg# plot (Fig. 2). Many of the sills are high in both Fe and Ti, similar to samples from propagating rifts (Christie and Sinton, 1986). However, considerable variations exist in Fe and Ti at the same Mg#. These variations must represent separate fractionation paths.

Trace Element Data

A plot of TiO_2 vs. Zr (Fig. 3) shows a roughly linear trend similar to the TiO_2 vs Mg# plot due to the strong control by fractionational crystallization. For any value of TiO_2, however, there is a range of values of Zr that cannot be related to differentiation. These variations must reflect multiple parental magmas resulting from a heterogeneous mantle source or, more likely, variable extent of partial melting of a single source region. The high Zr trend coincides with that of Site 858 and the low Zr trend coincides with that of Site 855. The values for Zr/Nb (15–57; Davis, Mottl, Fisher, et al., 1992) and Zr/Y (2.53–4.67) suggest that the sills include mostly normal (N-MORB) units with transitional compositions (T-MORB) in Units 10–12. Sills in Unit 8 (Zr/Nb = 29–30) and Unit 13 (Zr/Nb = 27) are also more enriched than the basalts from Sites 855 and 856.

The REE contents range from 10 to about 25 times chondrite, and form two groups (Fig. 4). Both are depleted in La relative to Ce with $[La/Ce]_n$ ratios of 0.73 to 0.99. One group has a flat middle and heavy REE pattern ($[Ce/Yb]_n$ <1; Fig. 3), but the other has a slight depletion in the heavy REEs ($[Ce/Yb]_n$ >1; Fig. 3). The only exception is found in the highly altered crosscutting dike in which Unit 10 shows a slight enrichment in La compared to Ce ($[La/Ce]_n$ = 1.01), possibly resulting from the extensive alteration or a different magma type. Eu depletion is notable in some samples, absent in others, and enriched slightly in a few plagioclase-rich samples, suggesting variable fractionation and accumulation of plagioclase within the sills. Samples with a negative Eu anomaly tend to show a more pronounced depletion in the LREE.

The data were examined stratigraphically in order to see if the sills form coherent groups or display any systematic variations with depth. On a plot of chondrite-normalized $[La/Yb]_n$ vs. depth (Fig. 9), several variations are evident. The data generally cluster into two groups, Group I, with $[La/Yb]_n$ greater than 1, and Group II, with $[La/Yb]_n$ less than 1. On the plot of this ratio vs. depth below seafloor, the two groups apparently alternate with depth. Within the lower Group II clusters, the data for closely spaced sills trend to lower $[La/Yb]_n$ with depth. No relationship between total REE content and depth is obvious at the scale of individual sills or clusters of sills, although the total REE contents appear to increase with depth below 600 mbsf. The position of each sill in Holes 857C and 857D was calculated using the logs for total gamma-ray counts and resistivity (Davis, Mottl, Fisher, et al., 1992). The sill contacts are identifiable within a few tens of centimeters, as the mafic rock is significantly less radioactive and more resistive than the adjacent sediment. These sills are plotted on a section showing the REE profiles (Fig. 10); the latter are positioned to reflect their approximate stratigraphic position. On this plot, several aspects are evident. Sills from the upper 50 m of Hole 857C (Core 139-857C-59R-1 to Core 139-857C-62R-2, Unit 1 to Unit 6; 450–500 mbsf) have generally flat patterns with LREE depletion in the lower members. Slight positive and negative europium anomalies occur within this horizon. Sills from the lower portion of Hole 857C (Core 139-857C-68R-1 to Core 857C-68R-3; Unit 7 to Unit 12; 500 to 570 mbsf) have flat REE patterns, with downward progressively larger negative europium anomalies with increasing depth. The only exception is the crosscutting dike (Unit 10), which is slightly enriched in LREE. Four sills from the top of Hole 857D (Core 857D-3R-1 to Core 857D-12R-1; Unit 14 to Unit 17, 570 to 700 mbsf) are LREE depleted, and have pronounced negative Eu anomalies. They are similar

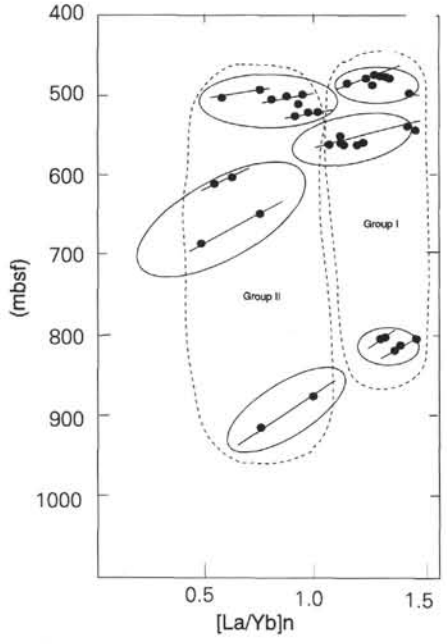

Figure 9. $[La/Yb]_n$ ratio vs. depth of samples from sills at Site 857 (chondrite normalized).

in total REE concentrations and REE patterns to the samples from Site 855. Sills below 700 mbsf (Core 857D-24R-1 to Core 857D-36R-1, Unit 21 to Unit 26) have flat patterns, with the sills below 850 mbsf (Cores 857D-32R-1 and 857D-36R-1, Unit 23 to Unit 26) displaying slight LREE depletion. The development of the negative Eu anomaly in the sills from 500 to 750 mbsf is indicative of removal of plagioclase from the melt. As the sills are quite thin (typically 10 m) and seemingly homogeneous (determined by petrographic examination, plus multiple samples from several of the sills, such as Unit 12, and others as shown in Fig. 10), this separation probably occurred in a shallow crustal magma chamber. The sill containing unusually calcic plagioclase and magnesiochromite (Unit 17) shows the largest negative Eu anomaly and the strongest depletion in the LREE. It is also one of the most altered, suggesting that the large Eu depletion may be due in part to plagioclase alteration. The values for $\delta^{18}O$ for this horizon (2.4–4.5‰) reflect the intense alteration of plagioclase and replacement by chlorite. The variable sample compositions suggest that the sills originated from at least two separate magmatic episodes or two small disconnected magma chambers.

Site 858, Holes F and G

Setting

The igneous units intersected at the bottom of Hole 858F were at a horizon considered too shallow for basement. However, the fine-grained nature of the rocks, the well-developed and ubiquitous variolitic textures, numerous chilled contacts, and the chemical uniformity of the basalt flows suggested to shipboard petrologists that this might be anomalously shallow basement — either a constructional high or an uplifted block adjacent to a buried basement fault. Drilling at Hole 858G was undertaken to determine the nature of the igneous unit and to penetrate as deeply as possible into igneous basement at an active hydrothermal area. Rare cherty pebbles were the only "sedimentary" material recovered within these holes below the basalt-sediment interface, supporting the interpretation that the drilling was into a topographic high comprised of extrusives.

All the igneous rocks recovered from Site 858 are basalt flows with variable quantities of tabular to columnar plagioclase, euhedral chro-

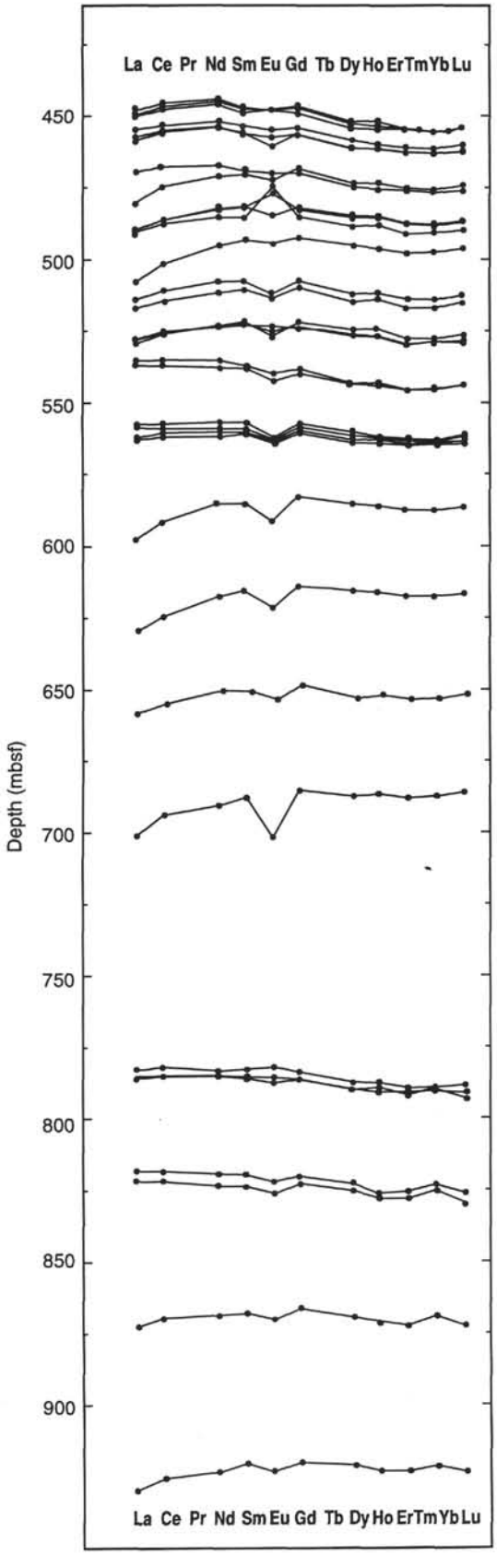

Figure 10. REE patterns plotted with depth in Holes 857C and 857D. Exact thickness of sill was determined from radiometric and resistivity logs, and is accurate to about 50 cm. Unit numbers are described in text.

mian spinel, and mafic silicates pseudomorphed by chlorite-smectite. Plagioclase is also present as a quenched phase with skeletal (lantern shapes and swallowtails on larger crystals) morphology. Much of the plagioclase is replaced by epidote and albitic plagioclase throughout both holes. The groundmass for most of the samples varies from cryptocrystalline or variolitic to microcrystalline, although no fresh glass is preserved. The only coarse-grained horizon is the basal unit for Hole 858G, which is a diabase (Sample 139-858G-16-1, 38–90 cm).

Petrography and Mineral Chemistry

The mafic phenocrysts are usually ovoid and replaced by a mixture of green to yellow pleochroic chlorite and smectite. The shapes of the pseudomorphs most clearly suggest olivine rather than pyroxene.

Spinel phenocrysts are dark red and commonly zoned with rims higher in Cr than the cores (Table 6; Fig. 5). The outer Cr-rich rim is conspicuous and frequently has inclusions of ilmenite and glass. The spinel phenocrysts are not uniformly present in the two Site 858 holes. They are common phenocrysts in the upper 40 m of basalt (from 249.9 to 288 mbsf) and in the lowermost basalt recovered from Hole 858G (413 to 423.7 mbsf). Small, sparse spinel crystals are also rarely noted at 296 mbsf and between 345 mbsf and 413 mbsf. Mg numbers vary from 0.35 to 0.75 and Cr numbers vary from 0.40 to 0.54 with one sample as high as 0.62 (Figs. 5C and 5D).

A few grains of ilmenite and magnetite were identified (Table 7, section B). These are small, anhedral, isolated blebs within the mesostasis. Magnetite is uniform in composition, with TiO_2 and Al_2O_3 contents typical of igneous rocks. Using the QUILF program (Anderson et al., 1993), an equilibrium temperature of about 800°C is indicated for the coexisting magnetite-ilmenite pair. This indicates that subsolidus equilibration of the oxide minerals was terminated at a fairly high temperature, although below expected eruption temperatures likely due to variable cooling of the basalt.

Plagioclase phenocrysts and microphenocrysts show strong optical and chemical zonation (Table 4). The most calcic phenocryst core compositions are An_{70-75}, except for Sample 139-858G-16R-1, 47–49 cm, which contains slightly more calcic plagioclase phenocrysts with core compositions of An_{76-80}. Microphenocrysts and groundmass plagioclase have more sodic compositions, similar in composition to sodic rims on the phenocrysts, An_{58-69}. Rarely, groundmass plagioclase is as sodic as An_{45}. Plagioclase commonly contains patchy replacement by albitic plagioclase, which is easily distinguished by the anomalous extinction and break in chemistry to An_{3-20}. Less commonly, plagioclase is partially replaced by epidote (Ps_{13-18}) analcime or prehnite, or even more rarely, by quartz and chlorite. The plagioclase compositions more calcic than about An_{45} are assumed to be primary.

Clinopyroxene is most commonly a granular to spherulitic groundmass mineral in the more crystalline samples in which Al_2O_3 contents vary from >4% to <2% (e.g., Sample 139-858-16R-1, 81–83 cm [piece 10]; Table 5). Where pyroxene is present as a phenocryst or microphenocryst phase it is typically higher in Ti than the associated groundmass phase.

Primary magmatic sulfides, such as those observed in samples from Site 856, are not present. Hydrothermal sulfides occur throughout most of the basalt samples from Holes 858F and 858G as small (0.1 mm), evenly dispersed grains of pyrite, pyrrhotite, chalcopyrite, and sphalerite, or as vein fillings.

Alteration

The basalts from this hole have been variably altered with a high preservation of the original texture. Alteration minerals were principally identified in pseudomorphs, veins, and vesicle fillings. The initial descriptions suggest that the rocks are less pervasively altered than those at Site 857, and that much of the secondary mineralization is related to vein and vesicle fillings rather than bulk replacement. The uppermost units contain low-temperature phases (e.g., calcite, smectite, and celadonite) that are overprinted by higher temperature phases (e.g., epidote, chlorite/smectite, and talc) in the deeper portions of the hole. The whole-rock values for $\delta^{18}O$ vary from 4.5‰ at the contact with the sediment to intervals only slightly depleted compared to fresh basalt (5.5‰) (Table 2). The sediment adjacent to the contact is similarly depleted in $\delta^{18}O$ ($\delta^{18}O = 6.1‰$) compared to the shallower sediment ($\delta^{18}O = 7.1‰$). The fine-grained basalt at the contact with sediment (Sample 139-858F-25R-1, 107–108 cm) is pervasively replaced by pale magnesian chlorite mixed with quartz. Plagioclase phenocrysts in this rock are replaced by epidote and albite, phases which also fill veins and vesicles. Prehnite also locally fills veins.

Sulfides are ubiquitous in the igneous rocks from Site 858 in quantities of 1%–5% (much less than at Site 857). They are present in veins with epidote, quartz, chlorite, prehnite, and wairakite. They also form ovoid porphyroblasts within the body of the rock by indiscriminately replacing igneous phases. Most sulfides observed are pyrite, with lesser quantities of chalcopyrite found with ferroan chlorite on fracture surfaces.

Geochemistry

The samples from Site 858 are remarkably uniform in composition (Table 1) and likely represent a single geochemical unit, although there are multiple cooling units. At least one chilled margin was recovered in each core (Davis, Mottl, Fisher, et al., 1992). Thus the whole-rock compositions are unlikely to be strongly modified by crystal accumulation. These are all altered somewhat, with H_2O contents of from 1.4 to 2.8 wt%, and total sulfur contents from 0.01 to 2.7 wt%. The H_2O content is not well correlated with any other element. Only the samples with the highest water content have elevated MgO contents. Ten samples form a "background" population with a median S content of about 0.1%, while the remainder form an "anomalous" population with a median content of about 0.9%.

Major Element Data

In selecting a suite of unaltered samples, we excluded all samples with total H_2O contents of more than 2.5 wt%, and total sulfur contents more than 0.7 wt%. This selection process eliminates samples that may have had significant additions or losses from or to either hydrothermal fluid or seawater. Eleven samples remain in this unaltered group.

The composition of the "unaltered" samples from this site are quite homogeneous. Their silica contents (46.90%–49.90%) are slightly less than those for samples from the other sites (855 and 857). TiO_2 (1.50%–1.61%) and Al_2O_3 (15.10%–16.40%) contents are similar to those for samples from Site 857. They are higher in Na_2O than the other sites, but have the same range of K_2O. The Site 858 basalts lie at lower values of Fe_2O_3T at the same Mg# compared to the other sites (Fig. 2).

The magnesium numbers of samples from Site 858 vary between 62 and 64, similar to samples from Site 857, but higher than at Site 855 and lower than at Site 856. Mg number based on spinel core composition (see Discussion) vary from 60–63, consistent with the whole-rock values.

Trace Element Data

The Ti vs. Zr trend parallels that of Site 857, but lies at higher values of Zr at the same Ti. The Zr/Nb values for basalts from Hole 858F are consistent (30–32) and classify these as N-MORBs similar to some of the sills with transitional character from Site 857.

The REE data illustrate the homogeneity of these rocks. The patterns are all similar, showing a slight depletion in La ($[La/Ce]_n$ = 0.84–0.94) and consistent depletion in the heavy REEs ($[Ce/Yb]_n$ >1.3) and a variably developed negative europium anomaly. In contrast, the $[La/Sm]_n$ is ≥ 1, suggesting transitional or enriched affinities. The high values for $[Ce/Yb]_n$ and $[La/Sm]_n$ compared to the other sites could result from a lower percentage of partial melting of the source. The negative Eu anomaly suggests that only about half of the

sampled flows show significant modification by fractionation of plagioclase. The single flow with a positive Eu anomaly suggests the accumulation of plagioclase phenocrysts, which is supported by petrography. The REE data are plotted in stratigraphic position in Fig. 11. The negative europium anomaly is not well developed in the uppermost and lowermost samples. The patterns are similar to those for basalts from the upper portion of Hole 857C (Cores 139-857C-59R-1 to -60R-1; Units 1 and 2).

DISCUSSION

Comparison of Phenocryst Data from the Four Sites

Although there is no fresh glass preserved in most of these samples, many of the mineral phases preserve their primary composition and can be used to infer magmatic history. The compositions of olivine and spinel in particular provide information regarding the composition of the primary magma at each drill site in spite of extensive hydrothermal alteration. During alteration, olivine is completely replaced and spinel alters to optically conspicuous ferritchromite, leaving no ambiguity regarding the primary character of the optically fresh phases. Pyroxene similarly preserves its primary composition unless conspicuously replaced by hydrous phases such as smectite or chlorite. Pyroxene compositions, however, are complicated by the presence of multiple generations, including megacrysts, phenocrysts, microphenocrysts, and quenched groundmass phases. In addition, the extended crystallization history of the sills at Site 857 has resulted in strongly zoned pyroxenes. Plagioclase similarly includes multiple populations. Primary variation in plagioclase composition is further complicated by alteration, which typically produces an increase in the sodium content of the primary mineral rather than a discrete, optically conspicuous replacement phase.

Spinel Compositions

Variations in chromian spinel compositions are extremely valuable in deducing the composition of primary magmas. The composition of the spinel can be directly related to the Mg# of the magma with which it equilibrated (Allan, in press). Spinel composition can be changed, however, under intense metamorphic conditions in which Mg may be preferentially removed to be incorporated into adjacent mixed layer clays (Allan, 1992). This would result in a large variation in Mg# with no covariation in Cr# (=Cr/(Cr + Al). The most Mg-rich specimens, spinels found as inclusions in fresh olivine or plagioclase and the core compositions of the spinels, can be credibly related to primary magma compositions. In general, spinel is more resistant to hydrous alteration than olivine, however, and provides the best estimate of the magmatic Mg# for sample suites in which no fresh glass is preserved.

Table 6 provides the calculated Mg# of the original magma host for each of the spinel compositions based on the algorithms of Allan (in press). The magma Mg numbers for the Site 856 spinel core compositions are extremely primitive, from 0.65–0.70. Groundmass spinel and rims on the larger grains are lower, varying from 0.50 to 0.62. The core Mg numbers are equivalent to or slightly higher than those of glass composition reported by Karsten et al. (1990) for magmas off the axis of the Endeavour Segment. The Mg numbers are similar to slightly higher than the primitive compositions reported by Leybourne and Van Wagoner (1991) for East Peak of the Heck Seamount Chain, although these latter magmas contain only sparse spinel. The spinel compositions are most similar to spinels compositions in samples from West Ridge as described by Van Wagoner and Leybourne (1991). The West Ridge magmas have been interpreted to have formed within Middle Valley when it was still the locus of spreading for this area but fresh primitive magmas from here have been interpreted as products of a more recent off-axis melting event (Van Wagoner and Leybourne, 1991).

The core composition for the single sample with spinel from Hole 857D overlaps the Site 856 composition (Mg# = 0.66) with lower values for the rim and groundmass spinel (Mg# = 0.65 and 0.63, respectively), suggesting a similarly primitive composition. Unlike Site 856, however, the sample from Site 857D contains calcic plagioclase megacrysts (An_{95-83}) and less aluminous spinel, indicating contemporaneous plagioclase and spinel formation, as also occurred at Site 858. Magmatic Mg numbers calculated from the Site 858 spinel core compositions range from 0.63 to 0.51, lower than those based on the spinel cores from Sites 856 and 857. Spinel rims suggest evolved magma compositions (0.49–0.52) with one Fe-rich spinel that indicates a magma Mg# of 0.41. Some of the spinels with calculated low Mg numbers from Site 858 also have low totals, which may suggest some effect of alteration.

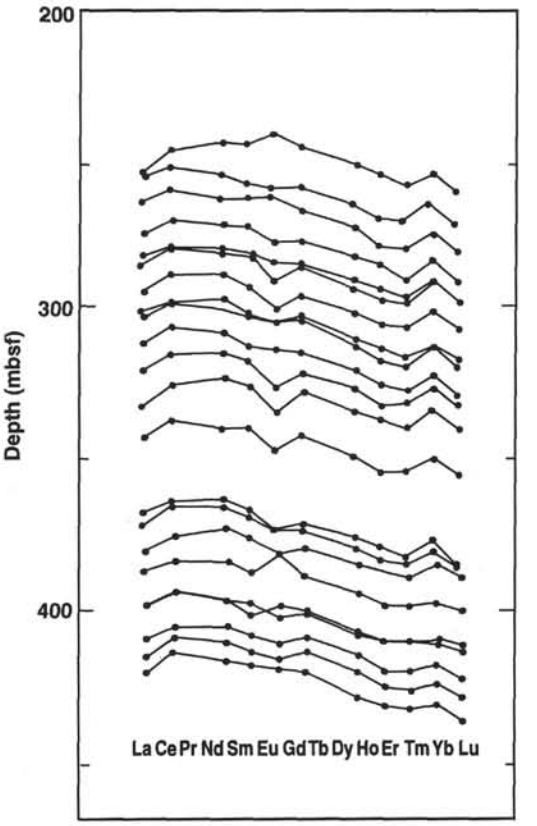

Figure 11. Chondrite-normalized REE patterns vs. depth below seafloor for basalts from Site 858.

Variations in the Cr# of the spinels are correlated both with primary magma composition and low pressure crystal fractionation. Primitive magmas with high Cr contents will contain spinels with both high Mg# and high Cr# inherited from the mantle source region. Spinels that crystallize from more evolved magmas would contain lower Cr contents and lower Cr# with lower Mg#. When plagioclase is present as a liquidus phase, however, the Al is preferentially included in this phase rather than the spinel. The result is a Cr-enriched rim with a low Mg# produced by plagioclase fractionation at low pressures (Allan et al., 1988). Figure 5E is a plot of Cr# vs. Mg# for spinels from Sites 856, 857, and 858. For a given lava suite derived from similar parental magmas, spinel Cr# increases and Mg# decreases with the amount of Fe-enrichment, Al depletion, and extent of fractionation (Allan et al., 1988). The core compositions for Site 856 are offset to a slightly higher Mg# than the spinels from Site 858, suggesting a more primitive magma. However, for spinel core compositions with the same Mg#, the Site 858 magmas are consistently higher in Cr. This suggests that these two magmas cannot be related by crystal fractionation. The single spinel found in one of the Site 857 sills plots in the center of the 858 population, though on the fringes of the 856 population, suggesting some affinity with the Site 858 magmas.

Zoning and complex skeletal rims are not found in either population of spinels, suggesting a simple magmatic history for both Site 856 and Site 858, without substantial magma mixing. The presence of the sharply defined Cr-rich (Al-poor) rim on a few crystals from Site 856 suggests some crustal fractionation of plagioclase. More extensive plagioclase fractionation for Site 857 and Site 858 is indicated by the lower aluminum content of the spinels compared to Site 856. Extensive fractionation is also indicated for the Fe-rich spinel in Site 858.

Oxides

The Fe-oxide compositions vary significantly between three areas (samples from Site 855 are too sparse to include). Site 856 contains groundmass titanomagnetite in addition to the rims on phenocrystic spinel. In contrast, Site 857 contains abundant ilmenite, indicative of the extensive crystal fractionation observed for some of the sills, but little modal magnetite or titanomagnetite. These latter phases may have been altered by the hydrothermal solutions, replaced by hydrous phases or by sulfide. The substantial addition of sulfur to the bulk rock compositions suggests that this latter process may be important. Variable Mn contents of the ilmenite may indicate differing extent of magma fractionation. Site 858 samples contain both ilmenite and magnetite, although neither is abundant. The moderate TiO_2 and Al_2O_3 contents of the magnetite distinguishes it from the hydrothermal magnetite in the sulfide deposit at Site 856, which is barren of these constituents. Ilmenite-magnetite pairs indicate relatively high (800°C) temperatures for the subsolidus equilibrium of these phases.

Olivine Compositions

Olivine is preserved in Site 855 and Site 856 samples. It is completely replaced in Site 858 samples and was likely present only in a few Site 857 samples. Olivine compositions for Site 856 (Fo_{88-90}) are considerably more magnesian than those at Site 855 (Fo_{83}). This is consistent with the primitive nature of the spinels present in the Site 856 basalts. Spinel is absent in the Site 855 basalts, perhaps as a result of a more extensive re-equilibration under crustal conditions. Neither group of olivine crystal contains significant zonation.

Plagioclase Compositions

The plagioclase in the Site 856 sills is more sodic than the plagioclase in the pristine Site 855 glassy basalts although the Site 856 olivines are more magnesian than those at Site 855. For Site 855, plagioclase phenocrysts are zoned from An_{90-85}, whereas groundmass or microphenocrystic plagioclase is An_{78-70}. At Site 856, in contrast, the plagioclase compositions vary from An_{78-64}, including the large phenocrysts or megacrysts with conspicuous oscillatory zoning. This could be due to magma mixing or the inclusion of crystals in a mush into a younger primitive magma, since more calcic compositions would be consistent with the appearance of spinel and olivine. Plagioclase phenocrysts in basalts from Site 858 are similarly sodic in composition, with the largest phenocrysts having core compositions of An_{70-75}, with only one sample as calcic as An_{80}. As the alteration of plagioclase in the Site 858 samples is dominated by replacement by albite or epidote, these sodic compositions are considered primary. The more sodic plagioclase in basalts at Site 856 and 858 compared to Site 855 could point to a later appearance of plagioclase in these magmas, more extensive fractionation, or to a deeper source region that produces more sodic magmas that those at Site 855. The lack of a significant Eu anomaly for either the Site 856 or Site 858 magmas argues against extensive low-pressure crystal fractionation. The plagioclase in the sills from Site 857 shows extreme variation from An_{73-43} in a single sample. Another single sample contains highly calcic plagioclase phenocrysts (An_{95}) zoned to a more moderate composition (An_{83}). Because of the strong within-sample zonation, it is not possible to correlate average plagioclase composition with other geochemical parameters except in the sample with extremely calcic compositions.

The sodic plagioclase compositions in these sills could be a result of extensive fractional crystallization within the coarser portions of the sills or the result of hydrothermal alteration. The abundance of chlorite suggests that some of the sodic plagioclase could be secondary, at least the conspicuous white sodic rims on the larger crystals. This is supported by depleted oxygen isotope analyses. It is likely that in-situ differentiation and alteration both play a role in determining the plagioclase composition.

Clinopyroxene

Clinopyroxene compositions show a broad range among the four suites of rocks. Megacrystic clinopyroxene is characterized by higher Al and Cr contents and lower Ti and Fe contents. The large rounded megacrysts at Site 855 are good examples of this (Table 5). Pyroxenes of such compositions are also found within the Site 857 sills as cores for the large crystals that enclose plagioclase. Rim compositions of these poikilitic crystals are normal augite to subcalcic augite, once again reflecting the extreme crystal fractionation of the coarse sill interiors. High Ti pyroxene is also found as brownish rims on pyroxene phenocrysts. All compositions of pyroxenes were found in some sections, suggesting mixing of magmas from different sources. Anhedral groundmass clinopyroxene also tends to have high Al contents, but low Cr and variable Ti. The aluminous groundmass pyroxene composition is assumed to reflect a quench effect. Site 856 only contains pyroxene as a groundmass phase. Most of the pyroxene at Site 858 is a groundmass phase, although some phenocrystic clinopyroxene was observed. The holocrystalline units at the base of Hole 858G contained pyroxene with both high and low Al. The paucity of pyroxene in the basalts from Site 856 and 858 point to the relative unfractionated nature of these magmas when they were intruded or extruded, although they represent different initial magma compositions.

Sulfide

Only the sills recovered from Site 856 contain sulfides that appear to be magmatic in origin. These are polysulfide aggregates of Ni-rich pyrrhotite with inclusions of pentlandite and chalcopyrite associated with plagioclase phenocrysts. The preservation of these delicate magmatic sulfide inclusions suggests that the Site 856 sills were little affected by hydrothermal circulation and must, as a result, postdate the event that produced the massive sulfide deposit at this site. The extraordinarily abundant sulfides in Site 857 are all hydrothermal in origin and represent a significant enrichment of S in the crust.

Relationship of Different Magma Types from Different Sites

Site 855 is composed of olivine-bearing, slightly altered tholeiite, typical of basalt elsewhere on the northern Juan de Fuca ridge and most similar to basalts described for south of the Cobb offset (Karsten et al., 1990). The refractory phenocrysts appear to be megacrysts not in equilibrium with the fresh glass host. These include forsteritic olivine, aluminous Cr-rich clinopyroxene and calcic plagioclase. The refractory phenocrysts are similar in composition to megacrysts in basalts from slow and intermediate spreading ridges such as the Mid-Atlantic Ridge (Stakes et al., 1984), and Costa Rica Rift (Natland, 1980; Natland et al., 1983) and reflect compositional variations associated with a fractional crystallization of plagioclase, 3–6 km depth (e.g., negative europium anomaly in most fractionated samples). The refractory compositions of the megacrysts and their corroded or rounded morphology suggests resorption of these phases during ascent or possibly mixing of relatively primitive and evolved magmas. Site 855 basalts form a linear trend on a Zr vs. TiO_2 plot and are LREE-depleted $[La/Sm]_n$ <0.7; $[Ce/Yb]_n$ <1.0). The major element contents, phenocryst compositions, and REE patterns are typical of normal MORB, suggesting that these samples are comagmatic and

correlated to three-phase crystal fractionation in a robust magma chamber. These compositions are likely the oldest for the Leg 139 suite as they represent basement further from the spreading axis.

Site 856 has primitive picritic basaltic sills, with abundant Cr-rich spinel and forsteritic olivine. The Mg# of the original magma can be deduced from the fresh spinel, which suggests magnesian compositions (Mg# 65–70). The spinel compositions are most similar to those found in the primitive magmas on West Ridge (Van Wagoner and Leybourne, 1991). These are among the most primitive compositions reported for the Juan de Fuca Ridge. The sills crosscut the sulfide deposits at Site 856 and therefore must postdate the main phase of hydrothermal deposition. Thus, they are the youngest samples collected. The REE patterns are depleted compared to the other sites and do not have Eu anomalies, once again pointing to magmas relatively unmodified by crustal processes. The compositions are strongly LREE-depleted ($[La/Sm]_n$ <0.4; $[Ce/Yb]_n$ <0.5). The patterns are similar to those for the Heck and Heckle Seamounts (Leybourne and Van Wagoner, 1991) and for anomalous late magmas on West Ridge (Van Wagoner and Leybourne, 1991). The aluminous compositions of the spinels suggest fairly deep origin for the spinels, although this is not diagnostic. Thus these sills represent an episode of magmatism with little modification at crustal depths, postdating the existence of a robust Middle Valley magma chambers.

The sills at Site 857 are extensively modified by hydrothermal alteration, which has substantially increased the volatile, sulfur, and magnesium contents of the whole-rock compositions. Strongly zoned plagioclase could have originated through extensive in-situ differentiation or hydrothermal alteration, although the paucity of albite suggests that the former process is most important. Variable clinopyroxene compositions and the appearance of ilmenite as the dominant Fe-oxide similarly point to extensive differentiation. Some of the sills, however, also contain accumulated refractory clinopyroxene megacrysts identifiable only by the core compositions of poikilitic crystals. These are similar in composition to the megacrysts in the Site 855 basalts.

Trace elements suggest that the sills were fed by multiple magma sources with both N-MORBS and T-MORBS found within the two deep drill sites. LREE-enriched and LREE-depleted compositions alternate stratigraphically. Both positive and negative Eu anomalies are noted, with the former associated with abundant plagioclase phenocrysts and megacrysts in the lower portion of the hole. Most of the sills, however, have negative Eu anomalies pointing to extensive crystal fractionation of plagioclase at crustal depths. The extensive crystal fractionation, large Eu anomalies and variable compositions suggests that these sills were fed by multiple small crustal magma chambers with separate fractionation pathways.

Three sills from the top of Hole 857D and one from Hole 857C have REE patterns and phenocryst compositions almost identical to the basalts from Site 855. These N-MORBs have the greatest depletions in LREE ($[La/Sm = 0.51–0.55]_n$), flat middle to heavy REE pattern and the largest Eu anomalies pointing to crystal fractionation of plagioclase. Calcic feldspars are found with Cr-rich spinel in one of these, suggesting the input of at least one new parental magma. These sills at Site 857 appear to have been derived from a mantle source region similar to that of Site 855. The other sills at Site 857 show either a smaller LREE depletion, a flat REE pattern, or even a slight enrichment in LREE. The sills from Hole 857D are dominated by this second magma type with $[La/Sm >1]_n$ and $[La/Ce]_n \approx 1$. The other sills are intermediate in composition between these two types. This suggests that the sill complex must have been fed from at least one other mantle source besides the depleted mantle that fed the Site 855-type magmas. Site 858 basalts are extrusives that form a constructional basement high. They are compositionally homogeneous and contain small amounts of quench plagioclase and Cr-rich spinel with compositions suggesting Mg numbers for the magma ranging from 60–63. The Site 858 basalts are characterized by $[La/Ce]_n$ values <1, $[La/Sm]_n$ values >1, and HREE depletions. The spinel compositions are similar to spinel in basalts from West Valley, the axial segment formed by rift propagation to west of Middle Valley, and overlap the composition found in the spinel-bearing Site 857 sill. This suggests that the Site 858 rocks are slightly enriched magmas from an axial seamount that formed during the final stages of magmatic activity in Middle Valley, feeding the sills at the adjacent Site 857. This second magma type may have mixed with the Site 855 N-MORB magma type to produce the intermediate compositions that dominate the sills in Hole 857D. The crosscutting dike found in Core 139-857C-66 was apparently of this composition.

CONCLUSIONS

Igneous rocks drilled during Leg 139 span the waning stages of the Middle Valley axial magmatic activity. The diversity of magmatic types represent (1) cogenetic magmas that have undergone different degrees of differentiation; (2) magmas derived from different source regions or variable partial melting; (3) mixtures of contemporaneous magmas; and (4) magmas that were not contemporaneous. The oldest magmas are the N-MORBS from Site 855, with chemistry and petrology typical of slow to medium spread ridges. Magmas from a similar mantle source region fed many of the sills found at Site 857, including the most altered (and presumably the oldest). These are characterized by $[La/Ce]_n$ <0.9, $[Ce/Yb]_n$ <0.9, and large negative Eu anomalies. A different mantle source region was tapped to produce the T-MORBs that constructed the topographic high at Site 858. These have $[La/Ce]_n \approx 0.9$ and $[Ce/Yb]_n$ >1.3. Magmas derived from this source also fed the sills at Site 857, with evidence of mixing between this magma and an N-MORB magma like that at Site 855. Postdating the main phase of axial magmatism, sills of primitive composition were intruded at Site 856. We conclude that the Site 856 sills represent primitive, off-axis magmas, the intrusion of which postdated the existence of a crustal magma chamber and its associated hydrothermal system. Their similarity to the seamounts and the off-axis magmas on West Ridge suggests that these rocks are the youngest in Middle Valley and may be associated with the failure of the Middle Valley spreading axis, contemporaneous with or postdating the jump of ridge axis activity to the adjacent West Valley. The differing compositions of Site 855 and Site 858 reflects either differing mantle source regions or a lower degree of melting for the latter, producing the higher values of $[Ce/Yb]_n$. For the Site 857 sills the $[La/Ce]_n$ is <1 regardless of the $[Ce/Yb]_n$, suggesting control by variable melting of a single source. Radiogenic isotopes are needed to assess this latter model (e.g., Frey et al., 1993). When the spreading jumped to West Valley, extensive crystal fractionation in small magma chambers with these mixed magmas created the highly evolved compositions in the other sills found at Site 857. The last phase of rift failure was marked by the eruption of the highly primitive lavas at Site 856.

ACKNOWLEDGMENTS

The authors would like to thank James Natland, Bryan Cousens, Matt Leybourne, and an anonymous reviewer for extensive reviews of an earlier version of this manuscript. This work was supported by a grant from JOI-USSAC to DSS and by the Geological Survey of Canada.

REFERENCES*

Allan, J.F., 1992. Cr-spinel as a petrogenetic indicator: deducing magma composition from spinels in highly altered basalts from the Japan Sea, Sites 794 and 797. *In* Tamaki, K., Suyehiro, K., Allan, J., McWilliams, M., et al., *Proc. ODP, Sci. Results,* 127/128 (Pt. 2): College Station, TX (Ocean Drilling Program), 837–847.

* Abbreviations for names of organizations and publications in ODP reference lists follow the style given in *Chemical Abstracts Service Source Index* (published by American Chemical Society).

Allan, J.F., in press. Cr-spinel in depleted basalts from the Lau Basin backarc, ODP Leg 135: petrogenetic history from Mg-Fe crystal-liquid exchange. *In* Hawkins, J., Parson, L., Allan, J., et al., *Proc. ODP, Sci. Results,* 135: College Station, TX (Ocean Drilling Program).

Allan, J.F., Sack, R.O., and Batiza, R., 1988. Cr-rich spinels as petrogenetic indicators: MORB-type lavas from the Lamont seamount chain, eastern Pacific. *Am. Mineral.,* 73:741–753.

Anderson, D.J., Lindsley, D.H., and Davidson, P.M., 1993. QUILF: a PASCAL program to assess equilibria among Fe-Mg-Ti Oxides, pyroxenes, olivine and quartz. *Comput. Geosci.,* 19:1333–1350.

Basaltic Volcanism Study Project, 1981. *Basaltic Volcanism on the Terrestrial Planets:* New York (Pergamon Press).

Christie, D.M., and Sinton, J.M., 1986. Evolution of abyssal lavas along propagating segments of the Galapagos spreading center. *Earth. Planet. Sci. Lett.,* 56:321–335.

Cousens, B.L., Chase, R.L., and Shilling, J.G., 1984. Basalt geochemistry of the Explorer Ridge, northeast Pacific Ocean. *Can. J. Earth Sci.,* 21:157–170.

Davis, E.E., and Lister, C.R.B., 1977. Tectonic structures on the Juan de Fuca Ridge. *Geol. Soc. Am. Bull.,* 88:346–363.

Davis, E.E., Mottl, M.J., Fisher, A.T., et al., 1992. *Proc. ODP, Init. Repts.,* 139: College Station, TX (Ocean Drilling Program).

Davis, E.E., and Villinger, H., 1992. Tectonic and thermal structure of the Middle Valley sedimented rift, northern Juan de Fuca Ridge. *In* Davis, E.E., Mottl, M.J., Fisher, A.T., et al., *Proc. ODP, Init. Repts.,* 139: College Station, TX (Ocean Drilling Program), 9–41.

Frey, F.A., Walker, N., Stakes, D., Hart, S.R., and Nielsen, R., 1993. Geochemical characteristics of basaltic glasses from the AMAR and FAMOUS axial valleys, Mid-Atlantic Ridge (36°–37°N): petrogenetic implications. *Earth Planet. Sci. Lett.,* 115:117–136.

Haggerty, S.E., 1976. Opaque oxide minerals in terrestrial igneous rocks. *In* Rumble, D., III (Ed.), *Oxide Minerals.* Mineral. Soc. Am., Short Course Notes, Hg101–Hg170.

Ito, E., White, W.M., and Göpel, C., 1987. The O, Sr, Nd and Pb isotope geochemistry of MORB. *Chem. Geol.,* 62:157–176.

Karsten, J.L., Delaney, J.R., Rhodes, J.M., and Liias, A., 1990. Spatial and temporal evolution of magmatic systems beneath the Endeavour Segment, Juan de Fuca Ridge: tectonic and petrologic constraints. *J. Geophys. Res.,* 95:19235–19256.

Klein, E.M., and Langmuir, C.H., 1987. Global correlations of ocean ridge basalt chemistry with axial depth and crustal thickness. *J. Geophys. Res.,* 92:8089–8115.

Langmuir, C.H., Bender, J.F., Bence, A.E., and Hanson, G.N., 1977. Petrogenesis of basalts from the FAMOUS area: Mid-Atlantic Ridge. *Earth Planet. Sci. Lett.,* 36:133–156.

Le Roex, A.P., Dick, H.J.B., Erlank, A.J., Reid, A.M., Frey, F.A., and Hart, S.R., 1983. Geochemistry, mineralogy and petrogenesis of lavas erupted along the Southwest Indian Ridge between the Bouvet Triple Junction and 11°E. *J. Petrol.,* 24:267–318.

Leybourne, M.I., and Van Wagoner, N.A., 1991. Heck and Heckle seamounts, northeast Pacific Ocean: high extrusion rates of primitive and highly depleted mid-ocean ridge basalts on off-ridge seamounts. *J. Geophys. Res.,* 96:16275–16294.

Mathez, E.A., 1980. Sulfide relations in Hole 418A flows and sulfur contents of glasses. *In* Donnelly, T., Francheteau, J., Bryan, W., Robinson, P., Flower, M., Salisbury, M., et al., *Init. Repts. DSDP,* 51, 52, 53 (Pt. 2): Washington (U.S. Govt. Printing Office), 1069–1085.

Michael, P.J., Chase, R.L., and Allan, J.F., 1989. Petrologic and geologic variations along the Southern Explorer Ridge, northeast Pacific Ocean. *J. Geophys. Res.,* 94:13895–13918.

Natland, J.H., 1980. Effect of axial magma chambers beneath spreading centers on the compositions of basaltic rocks. *In* Rosendahl, B.R., Hekinian, R., et al., *Init. Repts. DSDP,* 54: Washington (U.S. Govt. Printing Office), 833–850.

Natland, J.H., Adamson, A.C., Laverne, C., Melson, W.G., and O'Hearn, T., 1983. A compositionally nearly steady-state magma chamber at the Costa Rica Rift: evidence from basalt glass and mineral data, Deep Sea Drilling Project Sites 501, 504, and 505. *In* Cann, J.R., Langseth, M.G., Honnorez, J., Von Herzen, R.P., White, S.M., et al., *Init. Repts. DSDP,* 69: Washington (U.S. Govt. Printing Office), 811–858.

Papike, J.J., Cameron, K.L., and Baldwin, K., 1974. Amphiboles and pyroxenes: characterization of other than quadrilateral components and estimates of ferric iron from microprobe data. *Geol. Soc. Am. Abstr. Progr.,* 6:1053–1054. (Abstract)

Stakes, D.S., Shervais, J.W., and Hopson, C.A., 1984. The volcanic-tectonic cycle of the FAMOUS and AMAR valleys, Mid-Atlantic Ridge (36°47′N): evidence from basalt glass and phenocryst compositional variations for a steady state magma chamber beneath the valley mid-sections, AMAR 3. *J. Geophys. Res.,* 89:6995–7028.

Van Wagoner, N.A., and Leybourne, M.I., 1991. Evidence for magma mixing and a heterogeneous mantle on the West Valley segment of the Juan de Fuca ridge. *J. Geophys. Res.,* 96:16295–16318.

Date of initial receipt: 15 June 1993
Date of acceptance: 29 September 1993
Ms 139SR-212